Ocean Sci., 11, 699–718, 2015
www.ocean-sci.net/11/699/2015/
doi:10.5194/os-11-699-2015

Ocean Science
Open Access

Perspectives of transient tracer applications and limiting cases

T. Stöven[1], **T. Tanhua**[1], **M. Hoppema**[2], **and J. L. Bullister**[3]

[1]Helmholtz Centre for Ocean Research Kiel, GEOMAR, Kiel, Germany
[2]Alfred Wegener Institute Helmholtz Centre for Polar and Marine Research, Bremerhaven, Germany
[3]National Oceanic and Atmospheric Administration, Pacific Marine Environmental Laboratory, 7600 Sand Point Way NE, Seattle, WA 98115, USA

Correspondence to: T. Stöven (tstoeven@geomar.de)

Received: 18 August 2014 – Published in Ocean Sci. Discuss.: 16 October 2014
Revised: 6 August 2015 – Accepted: 21 August 2015 – Published: 18 September 2015

Abstract. Currently available transient tracers have different application ranges that are defined by their temporal input (chronological transient tracers) or their decay rate (radioactive transient tracers). Transient tracers range from tracers for highly ventilated water masses such as sulfur hexafluoride (SF_6) through tritium (^3H) and chlorofluorocarbons (CFCs) up to tracers for less ventilated deep ocean basins such as argon-39 (^{39}Ar) and radiocarbon (^{14}C). In this context, highly ventilated water masses are defined as water masses that have been in contact with the atmosphere during the last decade. Transient tracers can be used to empirically constrain the transit time distribution (TTD), which can often be approximated with an inverse Gaussian (IG) distribution. The IG-TTD provides information about ventilation and the advective/diffusive characteristics of a water parcel.

Here we provide an overview of commonly used transient tracer couples and the corresponding application range of the IG-TTD by using the new concept of validity areas. CFC-12, CFC-11 and SF_6 data from three different cruises in the South Atlantic Ocean and Southern Ocean as well as ^{39}Ar data from the 1980s and early 1990s in the eastern Atlantic Ocean and the Weddell Sea are used to demonstrate this method. We found that the IG-TTD can be constrained along the Greenwich Meridian south to 46° S, which corresponds to the Subantarctic Front (SAF) denoting the application limit. The Antarctic Intermediate Water (AAIW) describes the limiting water layer in the vertical. Conspicuous high or lower ratios between the advective and diffusive components describe the transition between the validity area and the application limit of the IG-TTD model rather than describing the physical properties of the water parcel. The combination of ^{39}Ar and CFC data places constraints on the IG-TTD in the deep water north of the SAF, but not beyond this limit.

1 Introduction

Ocean ventilation plays a major role in climate. It represents transport processes from the ocean surface to the ocean's interior, carrying dissolved gases, nutrients, and microorganisms, but also soluble hazardous substances and other coastal and offshore pollutants (Schlosser et al., 1999). One of the most prominent processes is the accumulative uptake of anthropogenic carbon (C_{ant}) at high and mid latitudes, where large volumes of surface and intermediate waters are transported into deeper water layers (e.g., Sabine and Tanhua, 2010). The excess uptake of atmospheric carbon dioxide (CO_2) by the ocean influences the marine ecology and biology, e.g., inhibiting shell building marine organisms due to acidification (Orr et al., 2005). Oxygen supply by ventilation represents another field of interest, with focus on the economically important marine resources like fish and seafood. To this end, ocean ventilation models are an important part of describing and understanding the complex biogeochemical interactions in the ocean.

A well-established concept is the transit time distribution (TTD) model that provides information about ventilation timescales and rates (Hall and Plumb, 1994; Bolin and Rodhe, 1973). The TTD model has several solutions and intended application possibilities. For example, the one-dimensional inverse Gaussian transit time distribution (IG-TTD) can be applied to field data of transient tracer surveys in the ocean (Waugh et al., 2003; Klatt et al., 2002).

An IG-TTD can be empirically constrained with a transient tracer couple that provides reliable mean age results of water masses in the ocean (e.g., Waugh et al., 2002; Schneider et al., 2012; Sonnerup et al., 2013; Stöven and Tanhua, 2014).

Here we present an overview of some commonly used transient tracers and their current specific restrictions on use with the IG-TTD. Section 2 highlights the power and weaknesses of each transient tracer, with a focus on the analytical and natural limits as well as other features. This section also includes figures of IG-TTD-based tracer time ranges and the resulting tracer order, which are shown to be indicative of the different characteristics of the transient tracers. Furthermore, a new method is proposed that allows for a fast and simple classification of the applicability of the IG-TTD to field data and that also describes the validity areas of the tracer couples. In Sect. 4, the new method of validity areas is applied to data sets from three transient tracer surveys. The transient tracer structure and limiting factors of the IG-TTD are presented and possible solutions to the determined restrictions are shown, e.g., the use of ^{39}Ar data in deep water. This work is an extension of the work by Stöven and Tanhua (2014), with the main focus on the future scope of IG-TTD applications.

2 Transit time distribution

2.1 Ventilation concept

Mixing processes in the ocean are difficult to quantify due to the various combinations of possible influencing factors. Hall and Plumb (1994) introduced a transit time distribution (TTD) model based on Green's function, which describes the propagation of tracer boundary conditions into the interior (Eq. 1), where $G(t)$ is Green's function and $c(t_s, r)$ the concentration of a transient tracer at year t_s and location r. The boundary concentration $c_0(t_s - t)$ is the concentration at source year $t_s - t$ related to the input function of a tracer. The exponential term accounts for the decay rate of radioactive transient tracers. Considering only the major components, like a steady and one-dimensional advective velocity and diffusion gradient, a practical model can be implemented, known as an inverse Gaussian transit time distribution (IG-TTD). This particular solution of the TTD can be stated as a simplified analytical expression (Eq. 2), where Γ is the mean age, Δ the width of the distribution and t the time range (Waugh et al., 2003). In the case of the IG-TTD, the location r is negligible because the distribution is compiled for every distinct sampling point of a tracer.

$$c(t_s, r) = \int_0^\infty c_0(t_s - t) e^{-\lambda t} \cdot G(t, r) \mathrm{d}t \quad (1)$$

$$G(t) = \sqrt{\frac{\Gamma^3}{4\pi \Delta^2 t^3}} \cdot \exp\left(\frac{-\Gamma(t-\Gamma)^2}{4\Delta^2 t}\right) \quad (2)$$

The Δ/Γ ratio of the TTD corresponds to the advective and diffusive characteristics of the fluid. Δ/Γ ratios < 1.0 describe a more advective water parcel, whereas ratios > 1.0 describe a more dominant diffusive share of the mixing process. A Δ/Γ ratio higher than 1.8 leads to large uncertainties in mean age and should be avoided (see below for more details). A Δ/Γ ratio of 1.0 is considered the unity ratio, which has been applied to many tracer surveys (Schneider et al., 2014, 2010; Tanhua et al., 2008; Waugh et al., 2006, 2004; Huhn et al., 2013). However, for more complex mixing structures, several approaches have been used to constrain the Δ/Γ ratio and thus the TTD-based mean age (e.g., Waugh et al., 2002; Schneider et al., 2012; Sonnerup et al., 2013; Stöven and Tanhua, 2014).

2.2 Transient tracers

2.2.1 Sulfur hexafluoride

Sulfur hexafluoride (SF_6) is an inorganic compound that was first synthesized in the beginning of the 20th century. It has been produced since the early 1950s on an industrial scale, mainly as insulating and quenching gas for high-voltage systems. The atmospheric sources are restricted to non-natural emissions by industrial plants. It is a highly inert gas with a very low degradation rate by UV radiation leading to an atmospheric lifetime of up to 3200 years (Ravishankara et al., 1993). Significant sinks besides ocean uptake are unknown or negligible. The SF_6 concentration of oceanographic data is stated in fmol kg^{-1} (fmol $= 10^{-15}$ mol). Since equilibrium concentration in surface waters depends on temperature and salinity, it is more appropriate to use the partial pressure of the tracer instead. It is stated in parts per trillion (ppt), which also allows a direct comparison with the atmospheric partial pressure. The current partial pressure in the atmosphere was ≈ 8 ppt in 2014, and this is increasing at a relatively constant rate (see Fig. 1). The use of SF_6 as a transient tracer in the ocean is restricted to well-ventilated water masses where the partial pressure is above the detection limit of the analytical system ($\approx$ 0.1 fmol kg^{-1} or ≈ 0.4 ppt at salinity 35 and potential temperature 4 °C). SF_6 has been used for deliberate tracer release experiments and as such there is potential for undefined offsets in concentrations in such survey areas and their surroundings (Tanhua et al., 2005, 2008).

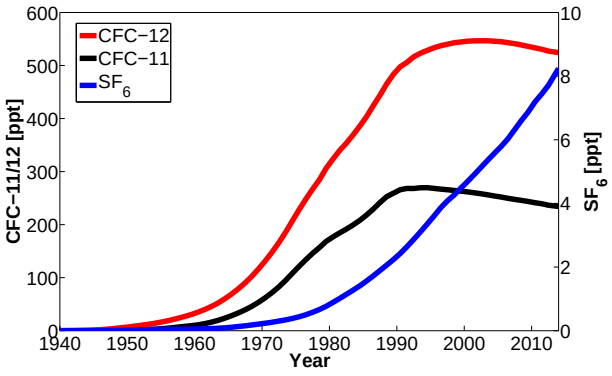

Figure 1. Atmospheric histories of CFC-12, CFC-11 and SF_6 of the Northern Hemisphere. The data were taken from Bullister (2015).

2.2.2 Chlorofluorocarbons

Chlorofluorocarbons, e.g., dichlorodifluoromethane (CFC-12) and trichlorofluoromethane (CFC-11), were originally produced for applications as refrigerants and were later also used as gas propellants. They are known as ozone-depleting compounds with atmospheric lifetimes between 90 and 130 years (Minschwaner et al., 2013). Production began in the late 1920s and was phased out in the late 1980s due to the infrared-mediated detrimental impact on atmospheric ozone concentrations. Hence, the observational record of the atmospheric CFC concentrations shows decreasing trends since the mid-1990s (Bullister, 2015). CFCs are only anthropogenically produced, and thus there are no sources within the ocean. CFC-12 has no significant sinks within the ocean, whereas CFC-11 has a minor sink by degradation in anoxic regions (Tanhua et al., 2005; Krysell et al., 1994; Lee et al., 1999, 2002). 1,2,2-trifluorotrichloroethane (CFC-113) and tetrachloromethane (by definition not a CFC, but included in this context) have possible sinks in the ocean at high temperatures and low oxygen concentrations that complicate the application as transient tracers. However, carbon tetrachloride may be useful in deep cold water where degradation is expected to be slow on decadal timescales. We assume that only CFC-11 and CFC-12 are sufficiently inert compounds and usable as transient tracers in all water masses of the ocean. The concentrations are stated in pmol kg^{-1} (pmol $= 10^{-12}$ mol) and the partial pressure in ppt. Upcoming problems are the decreasing concentrations in the atmosphere lowering the application range as transient tracers in the ocean (Fig. 1). Values above the current atmospheric concentration describe two dates in the atmospheric histories of the CFCs that lead to undefined results within age analyses such as the tracer age and the TTD-based mean age (see Sects. 2.4 and 2.6). This atmospheric concentration limit denotes the upper limit of use of CFCs, e.g., CFC-12 concentrations of 528 ppt in the Northern Hemisphere and 526 ppt in the Southern Hemisphere in 2014. The lower limit of use of CFC-11 and CFC-12 is set by the detection limit of, for example, $\approx$ 0.01 pmol kg^{-1} / $\approx$ 7.7 ppt at salinity 35 and potential temperature 4 °C.

2.2.3 Tritium

Tritium (^{3}H or T) is a radioactive isotope of hydrogen with a half-life of 12.32 years. It has a natural background concentration due to radiative-induced formation processes in the stratosphere and is usually oxidized to tritiated water (HTO). The extremely low concentration is commonly stated in tritium units (TU) where 1 TU is equivalent to 1 tritium atom per 10^{18} hydrogen atoms. The natural mean concentration in water vapor in air is 5.14 TU / 1.66×10^{-2} pCi mL^{-1} (1 pCi = 0.037 decays per second) and 0.49 TU / 1.6×10^{-3} pCi mL^{-1} in the ocean surface (Cossairt, 2012). The anthropogenic sources are nuclear facilities and the nuclear bomb tests during the 1940s, 1950s and mainly the 1960s where large amounts of tritium were released into the atmosphere with an estimated total activity of 2.4×10^2 Bq (CNSC, 2009). The tritium input into the ocean depends on precipitation, river input and water vapor pressure at the air–sea interface. Mean tritium input functions, e.g., the tritium input function of the Atlantic Ocean by Dreisigacker and Roether (1978) and Roether et al. (1992), imply uncertainties based on local differences of the net input. Thus it is difficult to obtain a generally valid tritium input function without neglecting prominent regional factors. For example, distinct local influences on the surface tritium concentration can be found in the Mediterranean Sea, which is characterized by a high net evaporation, large river runoff, dilution by Atlantic water and an intricate ventilation pattern (Roether et al., 2013; Stöven and Tanhua, 2014). Due to the possible uncertainties, it is recommended to use the tritium input function independent isotope ratio of tritium and the helium-3 ($^3He_{trit}$) decay product for TTD applications. The isotopic ratio is given in percent of the tritium decay and is stated as δ^3H in the following (Eqs. 3–4).

$$R = \frac{^3\mathrm{H}}{^3\mathrm{He_{trit}}} = \left(e^{\lambda t} - 1\right)^{-1} \quad (3)$$

$$\delta^3\mathrm{H} = \frac{R}{1+R} \cdot 100 \quad (4)$$

This method requires additional measurements of helium and neon to separate the tritiugenic share of the total ^{3}He concentration (Eq. 5). In this equation, $^3He_{tot}$ denotes the measured ^{3}He concentration in seawater, and $^3He_{ex}$ the excess ^{3}He, which can be determined with neon data and $^3He_{ter}$ as the terrigenic part, released by the earth's crust and mantle. The separation method is described by Roether et al. (2013). The terrigenic share has the most influence on the uncertainty because it cannot be directly determined. Possible estimates are graphical methods (Aeschbach-Hertig, 1994) and kine-

matic models (Roether, 1989), which have been developed for the helium–tritium dating method (Jenkins, 1977).

$$^3He_{trit} = {}^3He_{tot} - {}^3He_{eq} - {}^3He_{ex} - {}^3He_{ter} \quad (5)$$

2.2.4 Argon-39

Argon-39 (^{39}Ar) is a noble gas isotope with a half-life of 269 years. Similar to tritium, it is mostly formed by cosmic ray interactions in the stratosphere with ^{40}Ar as the main precursor. As a noble gas it is highly inert and there are no known sources or sinks in the ocean besides the radioactive decay. ^{39}Ar thus matches all requirements of a transient tracer. However, the measurement of ^{39}Ar is expensive, time-consuming and laborious. In contrast to CFCs, SF_6 and tritium, it is not possible to use the common way of water sampling with Niskin bottles. One of the first measurement systems for environmental samples was based on low-level decay counting (LLC) of 0.3–1 L of pure argon gas extracted from 1 to 3 tons of water per sample (Loosli, 1983; Schlitzer and Roether, 1985; Rodriguez, 1993). The concentration of ^{39}Ar is expressed as the isotopic ratio in water in relation to the isotopic ratio in the atmosphere (% modern). In spite of the obviously big stumbling blocks during sampling, and the enormous efforts that had to be put into the measurement facilities, the strong interest in this isotope and its scientific use have never ceased. Recently, a new method was developed to measure ^{39}Ar among other isotopes. The new technique is based on a laser-induced atom counting method, the so-called atom trap trace analysis (ATTA) (Jiang et al., 2011; Lu et al., 2014). This method allows for ^{39}Ar measurements from only 25 L of water down to an isotopic abundance of 8×10^{-16} (Jiang et al., 2011), which provides a possibility of measuring ^{39}Ar as part of transient tracer surveys in the ocean in the near future, thus significantly enhancing the modest current global data set.

2.2.5 Carbon-14

Carbon-14 (^{14}C), also known as radiocarbon, is a radioactive isotope with a half-life of $\approx$ 5730 years (Engelkemeir et al., 1949). The radiocarbon dating method, developed by W. F. Libby and co-workers (Libby, 1955), is a commonly used technique for dating carbon-containing material. However, this tracer is difficult to apply to the IG-TTD because of its indistinct boundary conditions at $c_0(t_s - t)$, i.e., the condition at the origin of the water parcel. This is caused by an alternating background concentration based on variability in the sun's activity (DeVries effect) and the earth's geomagnetic field (Stuiver, 1961). Furthermore, the massive burning of fossil fuels with low radiocarbon content has led to a dilution of the natural atmospheric concentration, i.e., the Suess effect (Tans et al., 1979), whilst nuclear bomb tests in the 1960s and nuclear fuel rod reprocessing have resulted in radiocarbon inputs to the atmosphere. Both effects, the dilution and the input of atmospheric radiocarbon, have their major origin in the Northern Hemisphere so that a gradient in ^{14}C occurs to the Southern Hemisphere. The third error source is the equilibration time at the air–sea boundary of almost 10 years that leads to a permanent disequilibrium at the ocean's surface (Broecker and Peng, 1974). Despite these problems, radiocarbon is a powerful tracer for water masses in the ocean, in particular those that are expected to be very old, e.g., in the deep basins of the northern Pacific.

Table 1. Detection limits of transient tracers. The presented values are approximate values that can deviate between different systems and the measurement conditions, e.g., lab or onboard measurements.

Tracer	LOD	Unit
CFC-12	0.01–0.001	pmol kg^{-1}
CFC-11	0.01–0.001	pmol kg^{-1}
SF_6	0.1–0.01	fmol kg^{-1}
^{3}H	0.02	TU
^{3}He	4.0×10^{-9}	^{3}He/^{4}He
^{39}Ar	8×10^{-16}	^{39}Ar/Ar
^{14}C	1×10^{-15}	^{14}C/C

Radiocarbon concentrations of oceanic measurements are commonly stated as Δ^{14}C in ‰ (Eqs. 6 and 7). The zero value of Δ^{14}C is defined by the used standard (usually AD 1950). Measurements are carried out with accelerator mass spectrometry (AMS). The detection limit of this technique is defined by an isotopic abundance of 10^{-15} (Krane, 1987) (Table 1) with a precision of 2–4.5 ‰. The sampling procedure is similar to the one of DIC samples described in Dickson et al. (2007) with a volume of 0.5 L and poisoning to inhibit biological activity during storage.

$$\Delta^{14}C = \delta^{14}C - 2\left(\delta^{13}C + 25\right)\left(1 + \frac{\delta^{14}C}{1000}\right) \quad (6)$$

$$\delta^{14}C = \left[\frac{(^{14}C/C)_{sample} - (^{14}C/C)_{std}}{(^{14}C/C)_{std}}\right] 1000 \quad (7)$$

2.3 Limit of detection

Transient tracer measurements in the ocean can be restricted by the detection limit of the used analytical system, which influences the application range of the tracer. The detection limits stated in Table 1 only represent common mean detection limits, since most measurements are carried out with a variety of custom-made analytical systems, sampling methods and sample volumes, which causes different detection limits. Furthermore, detection limits of onboard measurements are usually lower than under ideal laboratory conditions, and the methods of determining the detection limit also vary between the different working groups. For gas chromatographic systems, the detection limit should be stated as

3 times the standard deviation of the calibration blank (3σ), which is, for example, described by CLSI (2004). However, data far below the detection limit can be found in published data sets as a result of data calibration routines or offset corrections. The significance and the impact of systematic errors remain questionable and should be well discussed when using such data.

2.4 Tracer age

The tracer age (τ), also known as apparent age, has been used in the past to estimate the age of a water parcel. It is a simple approach that is described by a purely advective flow in the ocean, neglecting any mixing processes. It is also the lower limiting case of the IG-TTD for $\Delta / \Gamma = 0$. Equations (8) and (9) describe the tracer age for chronological transient tracers with $c(t_s)$ as the concentration at sampling year t_s and the referred atmospheric concentration $c(t_{hist})$ at year t_{hist}. The tracer age of radioactive transient tracers can be determined by the decay function (Eq. 10) with c_i as the initial concentration, c, the measured concentration and the decay rate λ. The tracer age of δ^3H depends on a decay function similar to Eq. (10), except that the equation is rewritten by using the decay product $^3He_{trit}$ instead of the initial concentration (Eq. 11).

$$c(t_s) = c_0(t_{hist}) \tag{8}$$

$$\tau = t_s - t_{hist} \tag{9}$$

$$\tau = \frac{1}{\lambda} \cdot \ln\left(\frac{c_i}{c}\right) \tag{10}$$

$$\tau = \frac{1}{\lambda} \cdot \ln\left(1 + \frac{\left[^3He_{trit}\right]}{\left[^3H\right]}\right) \tag{11}$$

Although the tracer age only provides approximate time information, it is still very useful as a generally applicable tracer unit since all the different concentration units can be directly related to a tracer age (Waugh et al., 2003). Another possible application is the so-called time lag analysis of CFC-12 and SF_6 (Tanhua et al., 2013). The basic principle is the similar growth rate of CFC-12 and SF_6 in the past with a time lag of ≈ 14 years. This means that a water parcel being steadily ventilated has the same tracer age based on SF_6 as it had ≈ 14 years earlier based on CFC-12. Therefore, differences between the SF_6 and CFC-12 tracer age indicate changes in ventilation. A slowing down of ventilation would lead to a higher, modern SF_6 tracer age and an increase in ventilation to a lower age compared to the historic CFC-12 tracer age. This method is clearly restricted by the availability of data sets covering the same region and the required time lag.

2.5 Time ranges

The specific time range of a transient tracer is essential when using field data within a TTD model and is defined by its input function and decay rate. The input functions of chronological transient tracers (CFCs, SF_6) are given by their atmospheric histories and information about surface ocean saturation trends. The input functions should exhibit a monotonic increase in tracer concentrations in the atmosphere for a proper applicability. Figure 1 shows the atmospheric histories of CFC-11/12 and SF_6 in the Northern Hemisphere. The recently decreasing trends of CFC-11/12 can clearly be seen, which cause restrictions of use (see Sect. 2.2). Data of atmospheric trace gas measurements at several locations in the world are provided by, for example, the AGAGE network with monthly updated data (Bullister, 2015). The distributed measurement stations are necessary, because most of the anthropogenic trace gases are released by the industrial nations in the Northern Hemisphere (see Fig. 9 in Bullister, 2015). Although the recent concentration gradient between the Northern Hemisphere and the Southern Hemisphere is small, significant differences of earlier years still persist in, e.g., North Atlantic Deep Water (NADW), Antarctic Bottom Water (AABW), and many more. Note that the hemisphere of the origin of the water parcel should be used rather than the hemisphere in which the sample was taken.

Natural radioactive transient tracers, such as ^{39}Ar, are independent of an input function due to a constant concentration level in the atmosphere, although deviations from saturation can occur. The formation processes of nuclides are usually radiatively initiated in the stratosphere and counterbalanced by the radioactive decay of the isotopes. Thus, natural isotopes are homogeneously distributed with relatively small variances in surface saturation in large parts of the ocean. An isotope meets the demand of an ideal tracer for the TTD method when there are no sources in the ocean and when a sufficient decay rate exists, serving as the only sink. Isotopes that are or were produced and released in the course of the operation of nuclear power plants or nuclear bomb tests might have a significant local or global input function into the ocean, which leads to several problems and restrictions in their use (see ^{14}C and ^{3}H in Sect. 2.2).

2.6 Mean age

For chronological transient tracers, such as CFCs and SF_6, the input function, the year of sampling and, to a minor extent, the hemisphere, are the required information for IG-TTD calculations. In contrast, radioactive transient tracer concentrations depend only on the decay rate (^{39}Ar) and some additional factors (^{3}H, ^{14}C; see above). The input function or decay-related concentration of a transient tracer is used as a boundary condition ($c_0(t_s - t)$ or $c_0\, e^{-\lambda t}$) to calculate theoretical tracer concentrations ($c(t_s, r)$) for a range of Δ / Γ ratios and a mean age spectrum (see Eq. 1). Figure 2

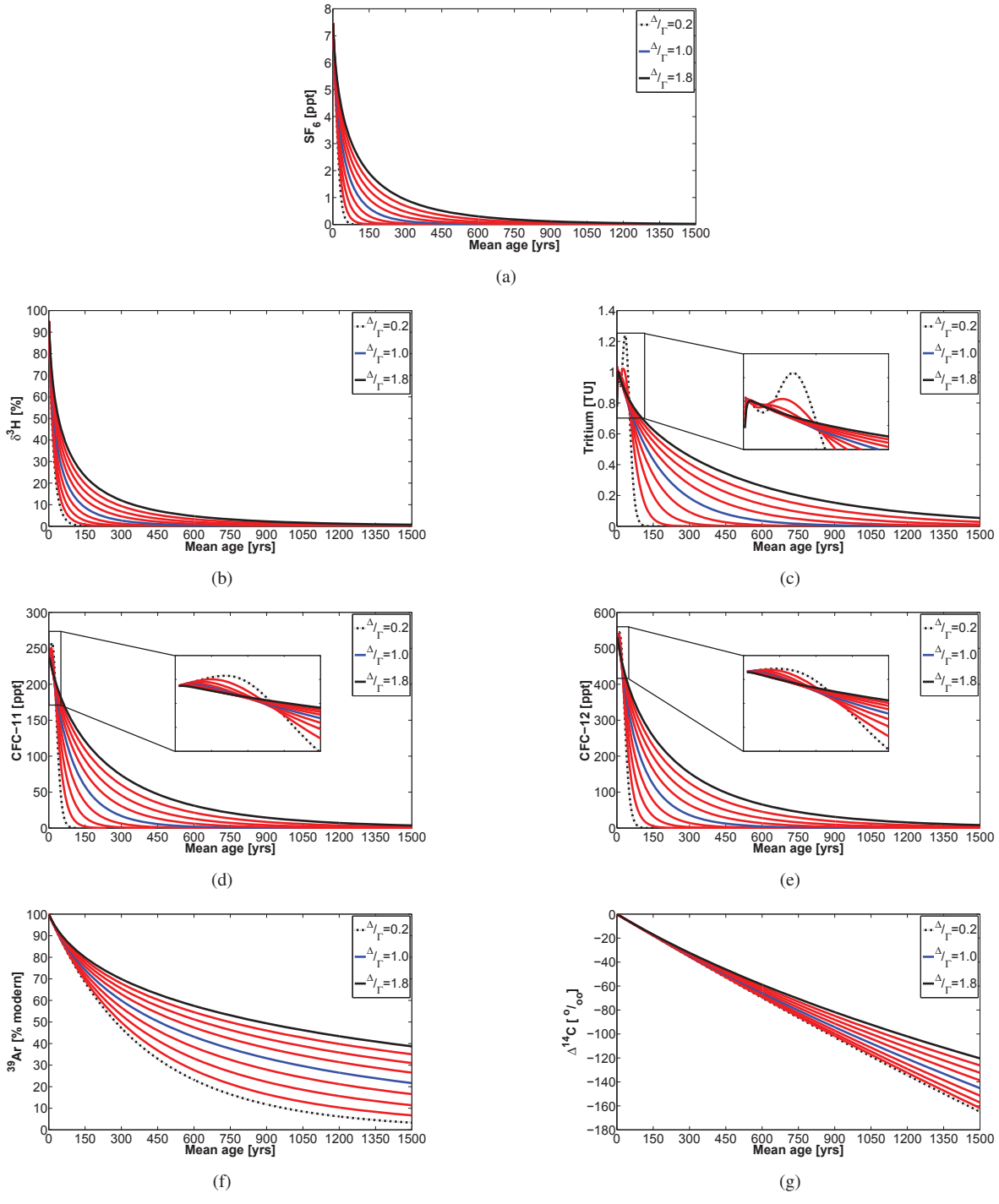

Figure 2. Transient tracer concentration of **(a)** SF_6, **(b)** δ^3H, **(c)** tritium, **(d)** CFC-11, **(e)** CFC-12, **(f)** ^{39}Ar, and **(g)** $\Delta^{14}C$ vs. mean age for different Δ / Γ ratios. The unity ratio of 1.0 is shown as a blue line and the lower and upper limits as dashed and solid black lines, respectively. The CFCs and tritium show a distribution anomaly that is caused by the decreasing atmospheric concentration of the tracers.

shows the model output of the different transient tracers. The theoretical tracer concentrations were calculated for Δ / Γ ratios between 0.1 and 1.8 and a mean age spectrum between 1 and 1500 years. The theoretical tracer concentrations can then be interpolated to measured concentrations ($c(t_{mes})$), which yields the different mean age results for the different Δ / Γ ratios. The IG-TTD model results of CFCs and ^3H show a sort of twist in lower mean age (Fig. 2c, d, e), which

is based on the declining trends of the atmospheric concentrations. Such a twist leads to a partly decreasing mean age with an increasing Δ / Γ ratio. However, it has no limiting influence on the IG-TTD model since it just describes the effect of a decreasing atmospheric tracer concentration. Note that the use of δ^3H shows no twist since it is independent of the tritium input function.

Related to possible age information, each tracer has a specific time and application range. Accordingly, the area between the Δ / Γ-ratio isolines indicates the application range of the tracer (Fig. 2). The bigger the difference between the isolines, the less sensitive are the results to deviations (errors) in measured concentrations and the more significant are the results. Figure 3 shows the relation between the relative tracer concentration in % and the tracer age, which highlights tracer similarities and the tracer order of the specific application ranges. The faster the tracer concentration declines, the smaller the time frame of application but the higher the time increment resolution. SF_6 and ^{3}H as well as CFC-11 and CFC-12 provide relatively similar time information. Application ranges of SF_6 and ^{3}H are younger to moderately old water masses, i.e., halocline and strongly ventilated water layers, which is indicated by the fast declining trend of both tracers. The application range of CFC-11/12 is restricted in shallower layers due to the atmospheric concentration limit, but provides time information for intermediate and deep water layers with significant ventilation due to deep water formation. Note that the tracer age at 100 % of CFC-11/12 is defined by the atmospheric concentration limit and is thus not equal to zero. ^{39}Ar extends the application ranges of CFC-11/12 due to the half-life of 269 years and the resulting slow decline of its concentration. Similar to SF_6 and δ^3H, it also has no restrictions besides the detection limit. The use of ^{14}C is restricted by the knowledge of the boundary conditions. A general TTD-based concentration can be calculated by using a boundary condition of $\Delta^{14}\mathrm{C} = 0$ so that the measured concentrations (related to a standard) just need to be converted to this scale. ^{14}C is a tracer for very old water masses ($\Gamma \gg 300$) and thus can be used in the time range of ^{39}Ar and beyond.

2.7 Constraining the IG-TTD

The shape of the IG-TTD (i.e., the Δ / Γ ratio) and thus the mean age can be constrained under certain assumptions using two transient tracers with sufficiently different time ranges. For example, SF_6/CFC-12 and CFC-12/^{39}Ar show clear differences in time ranges and tracer order (Fig. 3). Waugh et al. (2003) describes the characteristics of a tracer couple by using the relation between Δ and Γ for different tracer age isolines. The more the isolines differ from each other, the more useful the tracer couple. There are different methods described in the literature on how to constrain the IG-TTD, e.g., Waugh et al. (2002, 2004) and Schneider et al. (2012). Here we describe the method of Stöven and Tanhua (2014), which is based on intersections of mean age functions.

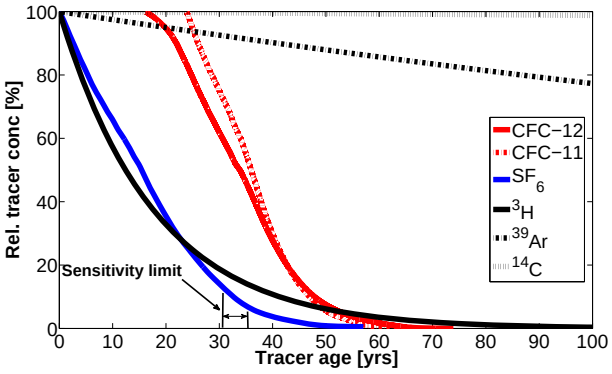

Figure 3. Tracer order based on the relation between the relative tracer concentration and the corresponding tracer age of 2012. SF_6 and ^{3}H as well as CFC-11 and CFC-12 show a similar behavior and cannot be used as tracer couples to constrain the IG-TTD. The sensitivity limit is explained in Sect. 4.4.

In the first step, the mean age of both tracers is calculated for each discrete water sample and a range of Δ / Γ ratios as described in Sect. 2.6. The mean age results of the corresponding Δ / Γ ratios can be expressed by a polynomial function of the second degree, which yields two mean age functions for each discrete water sample. The intersection of the mean age functions then describes the constrained mean age and Δ / Γ ratio; i.e., both tracers specify the same results. The sensitivity of this method to deviations in tracer concentrations is discussed below in Sect. 3.1.

3 The concept of validity areas

The specific characteristics of a tracer couple, such as the time range of application, limiting factors and other features of the IG-TTD, can be described by validity areas (grey shaded areas in Fig. 4). They are defined by the TTD-based tracer age relationship, which means that every distinct point within the area describes a tracer age relationship that belongs to a specific Δ / Γ ratio and mean age; i.e., the tracer age relationship is defined by the IG-TTD. For example, the isoline of $\Delta / \Gamma = 1.0$ (blue line in Fig. 4) is calculated by applying the concentration range of one tracer to the IG-TTD of this particular ratio. The determined mean age results are then used to back-calculate the theoretical concentrations of the second tracer (see Sect. 2.6), so that both tracer concentrations describe the same mean age. The tracer age relationship is then determined by recalculating both tracer concentrations to the corresponding tracer age.

The limits are defined by the detection limits of the tracers and the lower and upper limits of the IG-TTD. As stated above, the detection limits can vary within a certain range, so that the indicated limits for CFCs and SF_6 (dash dotted grey lines) only show an example of detection limits by Bullister and Wisegarver (2008). In addition to these upper tracer

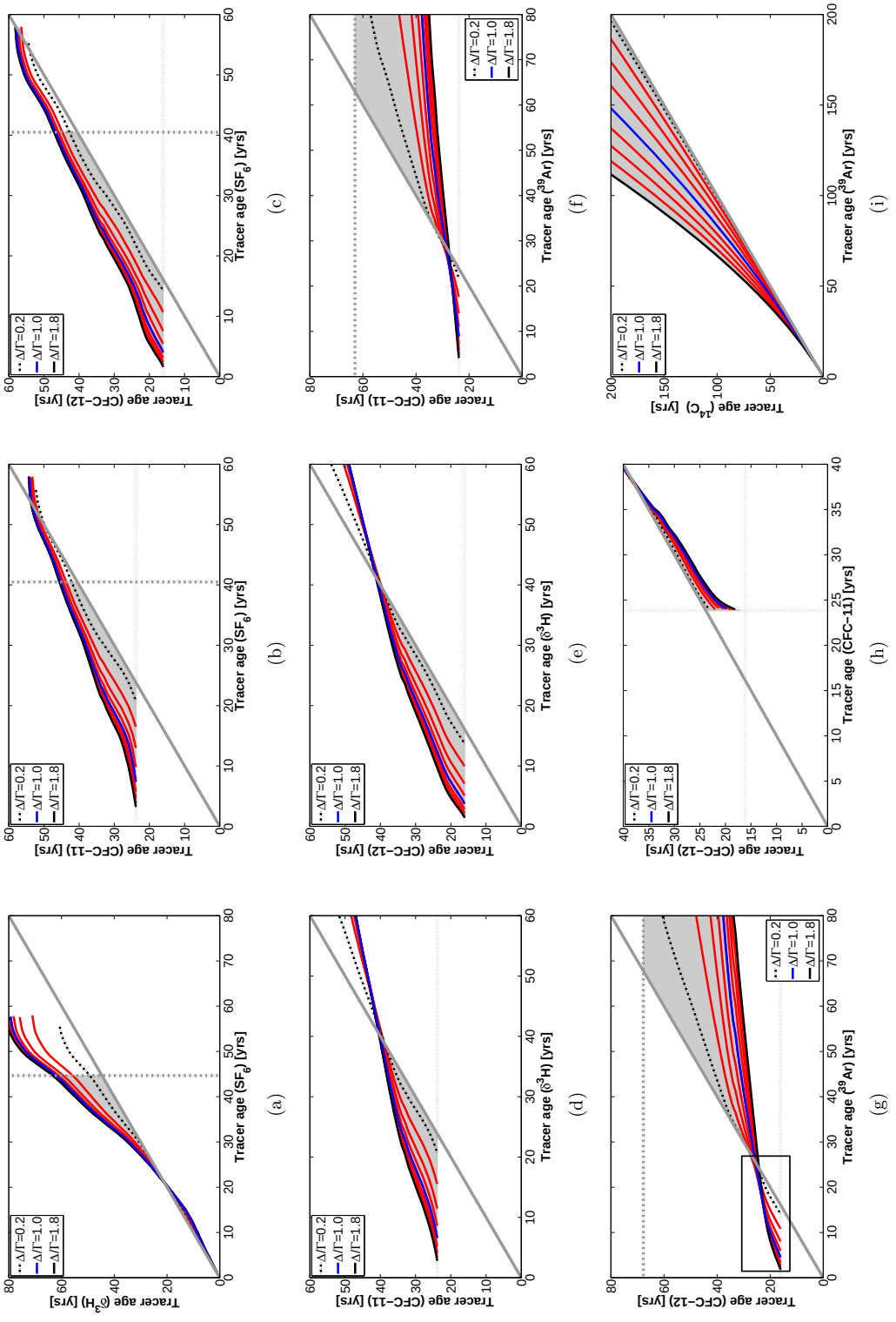

Figure 4. IG-TTD validity areas of the transient tracer couples using the tracer age relationship. The grey area describes the IG-TTD-based tracer age relationship for Δ/Γ ratios between 0 and 1.8 (see Sect. 3 for an explanation). Consequently, the boundaries are the bisecting line (grey solid line) with $\Delta/\Gamma = 0$, i.e., where both tracer ages are equal, the detection and atmospheric concentration limit of the tracer (dashed and dash dotted grey lines, respectively) and the IG-TTD-based tracer age relationship of $\Delta/\Gamma = 1.8$ (black solid line). The red solid lines indicate a Δ/Γ-ratio increment of 0.2. The tracer couples are **(a)** δ^3H/SF$_6$, **(b)** CFC-11/SF$_6$, **(c)** CFC-12/SF$_6$, **(d)** CFC-11/δ^3H, **(e)** CFC-12/δ^3H, **(f)** CFC-11/^{39}Ar, **(g)** CFC-12/^{39}Ar, **(h)** CFC-12/CFC-11 and **(i)** ^{39}Ar/Δ^{14}C. Areas with intercepting Δ/Γ isolines (black box in **g**) are indistinct in tracer age and thus non-constrainable.

age limits, the atmospheric concentration limit of the CFCs leads to a lower tracer age limit, reducing the size of the validity area (dotted grey line in Fig. 4b–h). The lower IG-TTD limit is defined by $\Delta/\Gamma = 0$, where $\tau_1 = \tau_2$ (solid grey line), which describes a purely advective flow. The upper IG-TTD limit depends on the chosen error range. The isolines of the Δ/Γ ratios in Fig. 4 are color coded as in Fig. 2. The red isolines in Fig. 4 clearly show a decreasing distance between each other for an increasing Δ/Γ ratio, with the only exception of the tracer couple ^{14}C–^{39}Ar. This means that the higher the Δ/Γ, the more sensitive the mean age for deviations in tracer saturation and tracer age. Therefore, we recommend a limit of $\Delta/\Gamma = 1.8$ (solid black line) for tracer couples including CFCs, SF_6 and δ^3H. The different sensitivities are discussed below in Sect. 3.1.

Intersections between the lower IG-TTD limit (bisecting line) with Δ/Γ ratio isolines and between the isolines themselves (black box in Fig. 4g) can be explained by a change in the tracer order (see curve intersections in Fig. 3). This causes an infinite number of indistinct tracer age relationships that are described by several Δ/Γ ratios. Consequently, these areas cannot be used to constrain the IG-TTD and are not part of the validity area.

Figure 4a and h show the validity areas for tracer combinations of δ^3H/SF_6 and CFC-11/12, i.e., combinations of tracers with a similar time range of application (see Fig. 3). Both combinations are examples of less adequate tracer couples, which is indicated by the small validity area and the small differences between the Δ/Γ-ratio isolines. This causes a high sensitivity to deviations in tracer age and thus high uncertainties in constraining the IG-TTD. In contrast, the remaining tracer couples provide significant information about Δ/Γ ratios in the range of their validity areas. The concept of validity areas can be used to determine the applicability of the IG-TTD by plotting the tracer age relationship of field data together with the validity area. Furthermore, the prevailing Δ/Γ ratios of field data within the validity area can simply be estimated (see Sect. 4.2).

3.1 Tracer saturation and TTD sensitivity

The unknown saturation state of CFCs and SF_6 at the time a water parcel was formed, i.e., when it lost contact with the atmosphere, constitutes the highest uncertainty in tracer applications (Shao et al., 2013). The equilibration time of the tracer, deep convection or subduction of surface waters, entrainment of subsurface water with low tracer concentrations, ice-covered areas, wind speed and sea surface temperature and salinity are all factors that influence the saturation state and can result in an undersaturated or supersaturated water parcel. Compared to systematic or analytical errors in the range of 2–3 %, the uncertainty of the saturation can be up to 60 % undersaturation (Haine and Richards, 1995; DeGrandpre et al., 2006; Tanhua et al., 2008; Shao et al., 2013). To this end, saturation is corrected with respect to the original approximate surface saturation of the water parcel. Shao et al. (2013) modeled the surface saturation of CFC-12, CFC-11 and SF_6 on a global scale with a monthly resolution up to the year 2010. The model output is provided at http://www.apl.washington.edu/project/project.php?id=cfc_mixed_layer and allows for various options of saturation corrections. The ideal correction of the saturation would be the specification of all involved source water masses, e.g., via optimum multi-parameter (OMP) analysis, which then provides information about the source areas and thus about the different degrees of saturation of the transient tracers. Complex water mass mixtures would probably entail a disproportionately high effort considering the gained reduction of uncertainty, and a mean saturation correction would be the more reasonable choice.

The constrained parameters of the IG-TTD, such as the Δ/Γ ratio and mean age, depend on the saturation ratio of the used tracer couple. Relatively similar deviations in tracer saturation lead to changes in mean age, but less in Δ/Γ ratios. Differences in the saturation state, in contrast, lead to significant changes in the Δ/Γ ratios, which is highlighted in Fig. 5. In this example we show the relative deviation of the Δ/Γ ratio and mean age for different saturation effects of the tracer couples CFC-12–SF_6 and CFC-12–^{39}Ar. In generating Fig. 5, the SF_6 and ^{39}Ar concentrations were kept constant for reasons of simplicity, so that the sensitivity of saturation ratios only depended on changes in CFC-12 concentration in the range of ±15 % difference in saturation. The initial points either vary in the Δ/Γ ratio (0.4, 0.6, 1.0, 1.4 and 1.8) for a constant initial CFC-12 concentration of 100 ppt (Fig. 5a, b, e, f) or vary in the CFC-12 concentration (100, 200, 300 and 400 ppt) for a constant initial $\Delta/\Gamma = 1.0$ (Fig. 5c, d, g, h). The corresponding initial concentrations of SF_6 and ^{39}Ar were determined by back-calculating the theoretical tracer concentration according to the method in Sect. 3. This means that the initial points also correspond to specific points (tracer age relationships) within the validity area in Fig. 4c and g. In these figures, a change in the CFC-12 concentration leads to a shift along the CFC-12 tracer age axis. The associated changes in Δ/Γ ratios and mean age are then illustrated by Fig. 5. The error of the Δ/Γ ratios 1.4 and 1.8 is partly not illustrated because the shape of the IG-TTD becomes extremely flat for Δ/Γ ratios > 2.5 and the used numerical integration method produced indistinct results above this limit.

Figure 5a and b show an increasing sensitivity of the Δ/Γ ratio and mean age to changes in the saturation ratio for increasing initial Δ/Γ ratios and constant initial concentrations of SF_6 and CFC-12. This can be explained by the increasing rate of change of the Δ/Γ ratios for an increasing CFC-12 tracer age (see Δ/Γ-ratio isolines in Fig. 4c). Given by the tracer couple of CFC-12/SF_6, an undersaturation causes negative and smaller errors compared to a supersaturation, which causes positive and larger errors in the Δ/Γ ratio and mean age. Looking at the initial ratio of

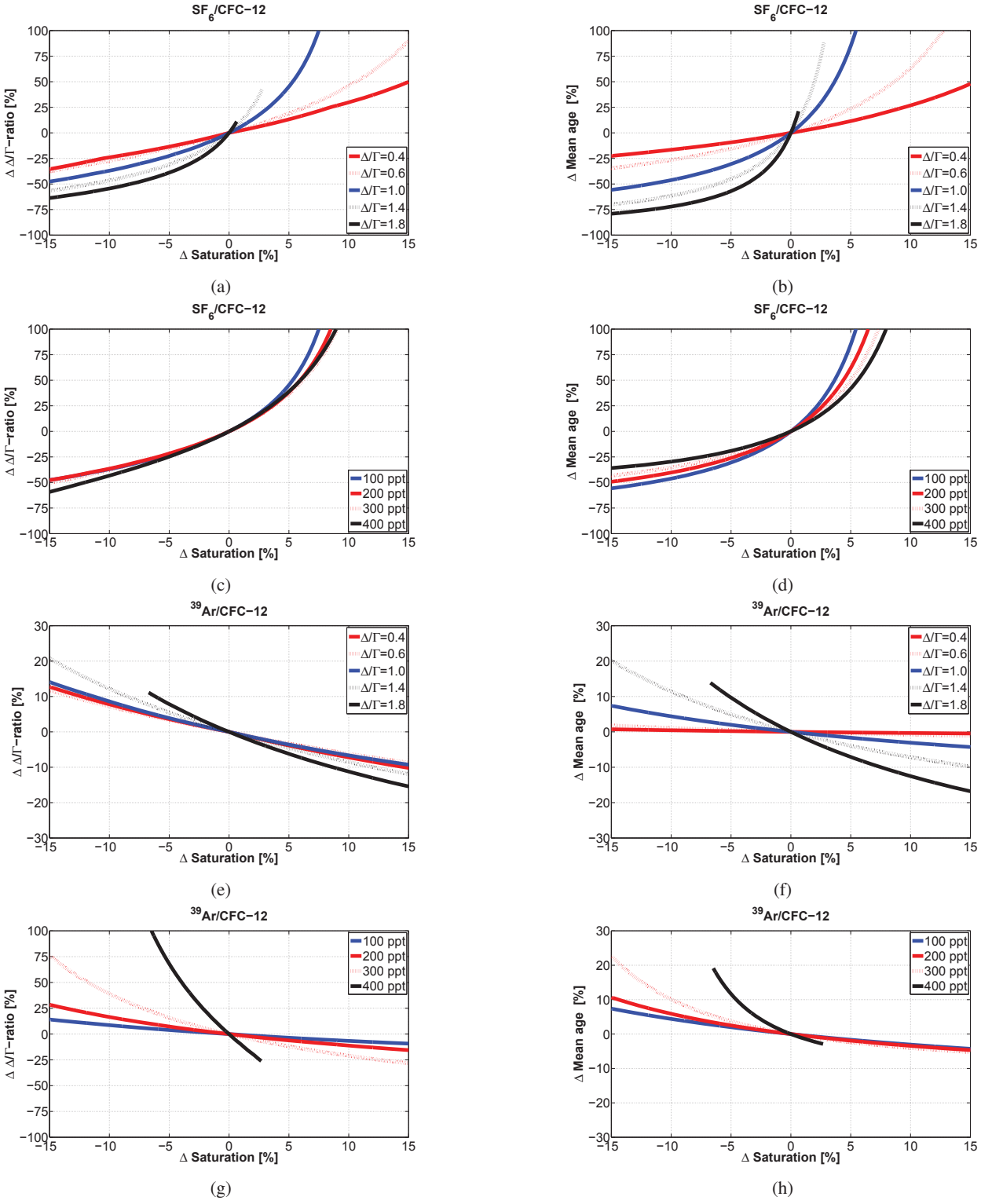

Figure 5. Δ / Γ ratio and mean age sensitivities to deviations in CFC-12 saturation based on the combination with **(a–d)** SF_6 and **(e–h)** ^{39}Ar. The sensitivities are shown for either a constant initial CFC-12 concentration of 100 ppt and a changing initial Δ / Γ ratio (**a**, **b**, **e** and **f**) or a changing initial CFC-12 concentration and a constant initial Δ / Γ ratio of 1.0 (**c**, **d**, **g** and **h**). The related tracer concentrations of SF_6 and ^{39}Ar are back-calculated by using the IG-TTD.

$\Delta/\Gamma = 1.0$ in Fig. 5a and b, which is a commonly used unity ratio, it can be seen that an undersaturation of 15 % causes a Δ/Γ ratio error of −47.6 % and a mean age error of −55.7 %. The same undersaturation causes an error of −63.8 and −79.1 %, respectively, for the initial ratio of $\Delta/\Gamma = 1.8$. Such CFC-12 saturation states occur frequently during water mass formation. Supersaturation is assumed to appear rarely in the ocean compared to undersaturation. However, only 5 % supersaturation would lead to an error of 45.2 % in the Δ/Γ ratio and 84.9 % in mean age for the unity ratio, and both can be expected to be far beyond 100 % for an initial ratio of $\Delta/\Gamma = 1.8$. The differences of sensitivities for changes in the initial CFC-12 concentration are less significant for Δ/Γ ratios with an error range of 50–60 and 15 % undersaturation (Fig. 5c). In contrast, Fig. 5d shows a clear trend with an increasing sensitivity of the mean age to decreasing CFC-12 concentrations from −35.9 to −55.7 % at 15 % undersaturation and from 41.8 to 84.9 % at 5 % supersaturation.

The differences in errors between the tracer couples CFC-12–SF_6 and CFC-12–^{39}Ar are due to the position of CFC-12 in the tracer order. SF_6 is ranked below and ^{39}Ar above CFC-12 (see Fig. 3). This generally means that changes in the concentration of the lower ranked transient tracer influences the TTD parameters in opposition to changes of the higher ranked transient tracer. Accordingly, the combination of CFC-12 and ^{39}Ar (with a constant ^{39}Ar concentration) leads to a reversal of the error signs and, furthermore, undersaturation now causes a higher sensitivity to both parameters than supersaturation. Figure 5e and f indicate that the tracer combination of CFC-12 and ^{39}Ar also leads to an increasing sensitivity of the Δ/Γ ratio and mean age for increasing initial Δ/Γ ratios, but yields smaller errors compared to CFC-12 and SF_6. However, low Δ/Γ ratios are less significant. This can be explained by the similar rate of change of Δ/Γ ratios of the different initial points (see $\Delta/\Gamma = 0.4$ in Fig. 5e). A CFC-12 undersaturation of 15 % results in a relatively low positive error of the Δ/Γ ratio between 10 and 15 % up to an initial $\Delta/\Gamma = 1.0$. The corresponding error of the mean age is also relatively low for $\Delta/\Gamma = 0.4$ with 0.7 % and $\Delta/\Gamma = 0.6$ with 1.8 %, but is significantly higher for higher ratios. Increasing initial CFC-12 concentrations from 100 to 300 ppt lead to increasing Δ/Γ ratio errors from 14 to 76 % and mean age errors from 7.4 to 22.8 % for an undersaturation of 15 %. Note that an initial CFC-12 concentration of 400 ppt is close to the limit of the validity area of the tracer couple, so that the error is partly undefined in the range of supersaturation.

We have demonstrated that the sensitivity of the IG-TTD parameters to changes in tracer concentration can be completely different, depending on the tracer couple. Furthermore, the results presented above are based on the limiting case that only one tracer differs in concentration (saturation), while the other remains constant. For the chronological transient tracers it is expected that occurring deviations from surface saturation apply to all tracers, although the magnitude will differ (Shao et al., 2013). It should be noted that the upper limit of the IG-TTD of $\Delta/\Gamma = 1.8$ is not arbitrary and fixed, but with respect to described problems above, an application of higher Δ/Γ ratios appears to be questionable.

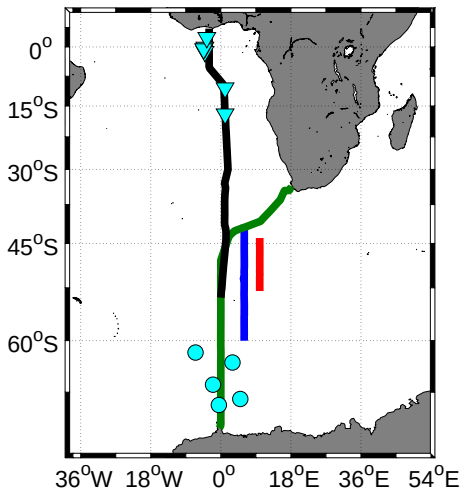

Figure 6. Sections of transient tracer surveys. The section of the ANT-XXVIII/3 cruise of 2012 is highlighted as a red line, the CLIVAR A13.5 cruise of 2010 as a black line, the SWEDARP cruise of 1997/98 as a blue line, the ANT-X/4 cruise as a green line and the ^{39}Ar data as cyan dots and triangles.

4 Field data applications

4.1 Transient tracer data

In the following we focus on data of less problematic transient tracers, namely SF_6, CFC-12, CFC-11 and ^{39}Ar, which have relatively well-defined input functions and represent different time ranges; i.e., they can be applied to well- and less well-ventilated water masses. The data sets were chosen to cover an area in the Southern Ocean, but for different years. We present a new data set of CFC-12 and SF_6 that was obtained during the ANT-XXVIII/3 expedition from 7 January to 11 March 2012 from Cape Town, South Africa, to Punta Arenas, Chile, on the German research vessel *Polarstern* (Wolf-Gladrow, 2013). The red line in Fig. 6 shows the sampling section along 10° E including 28 full-depth stations of CFC-12 and SF_6 measurements. The sampling procedure and measurement system (VS1) is identical as described in Stöven and Tanhua (2014). The data were corrected with 0.15 (±0.02) fmol kg^{-1} for SF_6 and 0.01 (±0.003) pmol kg^{-1} for CFC-12 due to a permanent offset of the ampule blank. The blank offset was continuously rechecked as part of the robust quality control routine described in Stöven (2011). Furthermore, the detection limit was sensitive to wave height changes, which had a direct impact on the baseline noise of the gas chromatograph. With increasing wave height, the baseline started to oscil-

late and became more noisy. The maximum elevated detection limit of 0.36 fmol kg^{-1} for SF_6 was observed during a storm with wind speeds of 20–25 ms^{-1} and a mean wave height of 8–9 m. The precision of the measurements was (whichever is greater) ±3.6 %/0.03 fmol kg^{-1} for SF_6 and ±0.8 %/0.015 pmol kg^{-1} for CFC-12. The data will be available at the Carbon Dioxide Information Analysis Center (CDIAC) database in October 2015.

The second data set (expo code: 33RO20100308) contains 129 stations with CFC-11, CFC-12 and SF_6 data that were obtained during the CLIVAR A13.5 expedition along the Greenwich Meridian in 2010 (black line in Fig. 6). The expedition took place from 8 March to 14 April from Cape Town, South Africa, to Takoradi, Ghana, on the American research vessel *Ronald H. Brown* (Bullister and Key, 2010). The measurement procedure can be found in Bullister and Wisegarver (2008). The precision of the measurements was 2 % or 0.02 fmol kg^{-1} (whichever is greater) for SF_6 and 1 % or 0.002 pmol kg^{-1} (whichever is greater) for CFC-11 and CFC-12 (Bullister and Key, 2010).

The third data set (expo code: 91AA19971204) containing CFC-12 and SF_6 data was collected during the SWEDARP expedition in January–February 1998 onboard the South African research vessel *S.A. Agulhas* (Turner et al., 2004). The section along 6° E includes 38 stations with a maximum depth of 3100 m due to the limited wire length on the winch. Two GC-ECD systems were used for onboard measurements where the SF_6 measurement system was similar to Law et al. (1994) and the CFC-12 measurement system to Grasshoff et al. (1999). The data, sampling and measurement procedure is discussed by Tanhua et al. (2004). The precision of the measurements was ±3.1 % or 0.06 fmol kg^{-1} (whichever is greater) for SF_6 and ±0.7 % or 0.03 pmol kg^{-1} for CFC-12.

The fourth data set (expo code: 06AQANTX_4) contains 98 stations with CFC-11 and CFC-12 data that were obtained during the ANT-X/4 expedition from 21 May to 6 August 1992 from Cape Town, South Africa, to Puerto Madryn, Argentina, on the German research vessel *Polarstern* (Lemke, 1994). The measurement procedure was similar to Bullister and Weiss (1988) and the data are discussed in Klatt et al. (2002) with a stated CFC-11 and CFC-12 precision of ±1.4 %/0.006 pmol kg^{-1} (whichever is greater) for CFC-11 and CFC-12.

Ocean data of ^{39}Ar were taken from Rodriguez (1993). The data include measurements of deep water masses in the eastern Atlantic close to the northern part of the A13.5 expedition and measurements in the whole water column near the southeastern end of the Weddell Sea (Table 2) during the 1980s and early 1990s. The sampling for one measurement was based on four 250 L Gerard Ewing samplers distributed over a depth range of 400 m so that every data point describes the corresponding mean value. The measurements were conducted at the University of Bern using the LLC method with a given relative error of 10–14 % (Schlitzer and Roether, 1985). The sampling and measurement procedure as well as data statistics are discussed by Loosli (1983) and Rodriguez (1993).

Table 2. ^{39}Ar data of the eastern Atlantic and southeastern Weddell Sea from the 1980s and early 1990s. The data are taken from Rodriguez (1993).

	Lat. (° N)	Long. (° E)	^{39}Ar (% modern)	pressure (dBar)
Eastern	−17	1.1	45	4440
Atlantic	−10.5	1.1	55	820
	−1.2	−4.1	42	4480
	−0.1	−4.1	67	1800
	−0.5	−4.4	53	2810
	2.4	−3.6	57	750
Eastern	−65.2	−2	46	245
Weddell	−65.2	−2	52	3055
Sea	−62.7	3	41	240
	−66.7	5	34	1245
	−67.3	−0.5	38	1990
	−61.5	−6.5	37	445
	−61.5	−6.5	44	675
	−61.5	−6.5	52	4070

4.2 Validity areas

The new method of validity areas, introduced in Sect. 3, allows for rapid determination of the application range of the IG-TTD. Figure 7 shows the application to the field data using the CFC-12–SF_6 and CFC-11–SF_6 tracer couples of three different cruises colored by the latitude of the sample station. The data were used unaltered for this approach, while the application of saturation corrections is discussed in Sect. 4.3 below.

For the SWEDARP data from 1998, about half of the data points are in the range of the IG-TTD (Fig. 7a). The data show a sort of randomly scattered structure rather than a clear trend, which is probably caused by low precisions of early SF_6 data. Nevertheless, it can be seen that most of the northern (red) data points are within the validity area and that most of the southern (blue) data points are above the upper limit of the IG-TTD. The transition zone is indicated by the mid-latitude (green/yellow) data points, which show the most scattered structure. Data points below the lower limit of the IG-TTD describe either an unusual relation between the saturation of both tracers or can be explained by measurement uncertainties. Note that the emission rate of CFC-12 was still slightly higher than the atmospheric degradation rate in 1998 and, thus, there is no atmospheric concentration limit. Figure 7b and c illustrate the validity area of the tracer couples CFC-12–SF_6 and CFC-11–SF_6, respectively, using the CLIVAR A13.5 cruise in 2010. Both tracer couples show the same trend up to a SF_6 tracer

age of ≈ 32 years. Beyond that, the data points are shifted towards higher Δ / Γ ratios and then beyond the IG-TTD limit the more southward the sample stations, similar to results obtained for the SWEDARP data. Comparison of the shape of the upper IG-TTD limit with the indicated shape of the scattered data points in Fig. 7c suggests that the tracer age relationship of the field data corresponds approximately to the IG-TTD-based tracer age relationship. In contrast, the data points for a tracer age > 32 years show a different structure. Data from the northern part (red data points) are shifted towards lower Δ / Γ ratios and the data from the southern part (blue data points) diverge in both directions whilst still remaining outside the validity area. Data above the SF_6 tracer age of 47 years correspond to SF_6 concentrations below the stated detection limit. Similar to the corrections of the ANT-XXVII/3 data, this can be explained by a calibration routine, which included a concentration offset so that negative SF_6 concentrations and concentrations below the detection limit were produced (see data information at CCHDO). Here, too, the application of such data is questionable due to the low significance. The ANT-XXVIII/3 data from 2012 are, except for a few data points in the lower age range, not applicable to the IG-TTD (Fig. 7d). Nevertheless, the same data trend, as determined from the SWEDARP and CLIVAR data, can be identified.

4.3 Saturation effects

The relative saturation state of transient tracer couples can cause large deviations in Δ / Γ ratios and mean age, which also influence the applicability of the IG-TTD. For reasons of convenience, only every third element of the CLIVAR data set was used. The degree of tracer saturation was obtained by calculating the mean surface saturation of the tracers using the model output from Shao et al. (2013). Since most of the water mass formations take place during winter, we used a 3-month mean centered around the month of maximum undersaturation. The area used for the calculations was selected to be 50–68° S and −30–20° E, which represents large parts of the Atlantic sector of the Southern Ocean. Figure 8 shows the results of this approach for CFC-11, CFC-12 and SF_6. The black and red stars in year 1992 correspond to the mean surface saturation of CFC-11 and CFC-12, based on the ANT-X/4 data that were obtained during austral winter in this region. This indicates that the model-based saturation approach possibly overestimates CFC undersaturations in particular regions, e.g., along the Greenwich Meridian. The yearly related saturation correction was applied to the atmospheric histories (boundary conditions) of the tracers, which led to changes in tracer age (Fig. 9). The red dots show the tracer age relationship of the uncorrected data and the arrowheads of the saturation-corrected data. The tracer age of all tracers is lowered, but significant changes, e.g., decreasing Δ / Γ ratios, can only be observed for a SF_6 tracer age < 20 years. This general trend can be explained by the counter-balancing effect of the similar undersaturation and the increasing sensitivity of the tracer age to high CFC concentrations. A relatively improbable correction based on undersaturation of CFCs and supersaturation of SF_6 would be necessary for most of the data to enable an application of the IG-TTD.

Interestingly, supersaturation of CFC-12 and SF_6 was observed during the ANT-XXVIII/3 cruise. Surface measurements a few hours after heavy wind conditions showed significant supersaturation of SF_6 (Fig. 10). The observed surface values were elevated above equilibrium concentrations for SF_6 ($\sim 2.7\,\mathrm{fmol\,kg^{-1}}$) and CFC-12 ($\sim 2.5\,\mathrm{pmol\,kg^{-1}}$) by about 20–50 and 2 %, respectively. The observed SF_6 and CFC-12 supersaturations are consistent with injecting and completely dissolving a few cc's of modern air ($SF_6 = 7.7$ ppt and CFC-12 = 526 ppt) into each kilogram of near-surface seawater. According to Liang et al. (2013), it can be assumed that bubble effects lead to elevated surface tracer concentrations during heavy wind conditions. The degree of supersaturation depends on the gas solubility; i.e., less soluble gases are more affected than soluble ones. This would explain the much higher supersaturation of SF_6 compared to CFC-12 in Fig. 10.

4.4 Application range of the IG-TTD

To investigate the different limiting factors of the IG-TTD, we used the CLIVAR A13.5 data set that provides transient tracer data from 5° N to 54° S along the Greenwich Meridian. The concentrations are shown in Fig. 11. The data were not interpolated to avoid a distortion of results due to the large share of data below the detection limit (indicated by black dots in Fig. 11). CFC-11 and CFC-12 show, as expected, a similar distribution. Concentrations below the detection limit and CFC-free water masses are found in the depth range below ≈ 1200 m between 10 and 30° S. Elevated CFC concentrations between 2 and 30 ppt of CFC-12 and between 1 and 16 ppt of CFC-11 characterize the intermediate and deep water below 1200 m in the northern part from 4° N to 7° S. In contrast, SF_6 shows only single data points above the detection limit (≈ 0.07 ppt) that seem randomly distributed in the deep water. This underlines the fact that measurements of SF_6 are still very challenging and that SF_6 applications with concentrations close to the detection limit do not provide robust results. South of 30° S, both CFCs can be detected in almost the complete water column. This is a result of the circulation pattern in the Southern Ocean (e.g., Whitworth and Nowlin, 1987), which transports tracer-rich water masses into the ocean's interior. The Antarctic Bottom Water (AABW) plays a major role in deep water ventilation. It is formed at the shelf regions of the Antarctic continent and propagates northwards along the bottom of the ocean. The CFC-12 bottom concentration decreases from 30 ppt at 54° S to 5 ppt at 30° S. The CFC-11 bottom concentration decreases from 16 to 2 ppt, whereas SF_6 shows no clear

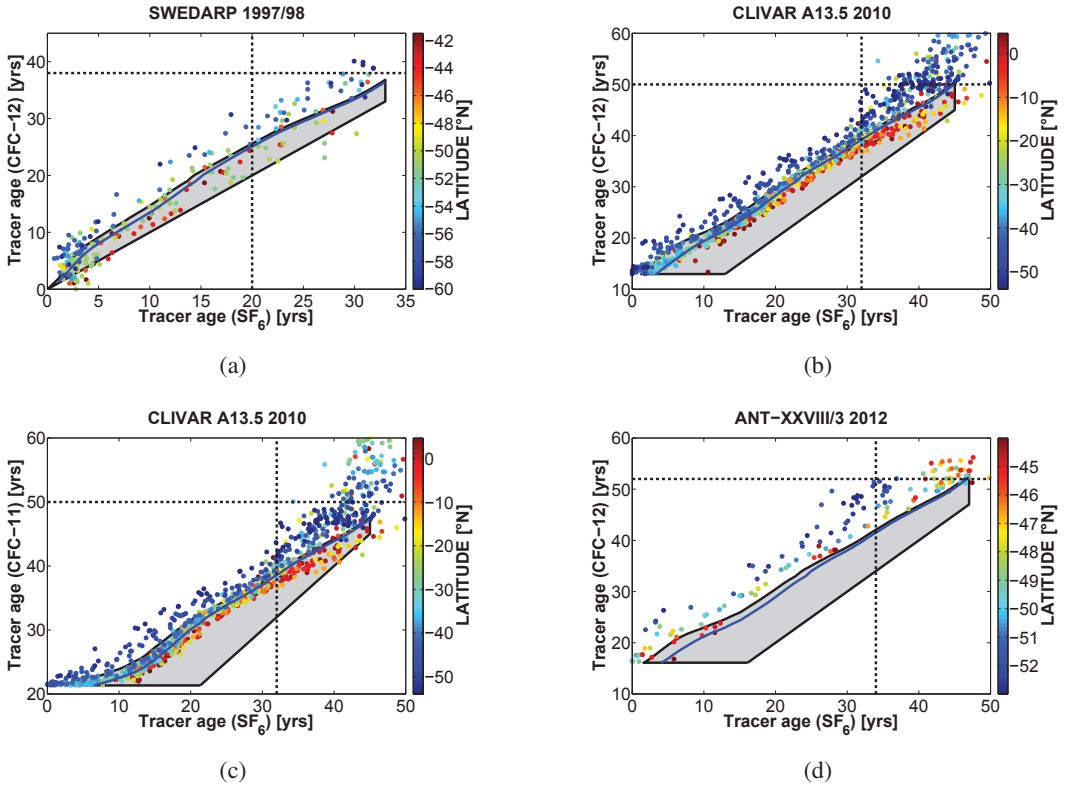

Figure 7. Validity areas (grey shaded area) and tracer age relationships of **(a)** CFC-12/SF_6 of the SWEDARP cruise of 1998, **(b, c)** CFC-12/SF_6 and CFC-11/SF_6 of the CLIVAR A13.5 cruise of 2010 and **(d)** CFC-12/SF_6 of the ANT-XXVIII/3 cruise of 2012. The data are colored by latitude from red (north) to blue (south); the blue line describes the tracer age relationship of the unity ratio $\Delta / \Gamma = 1.0$. The north–south trend of Δ / Γ ratios being shifted towards the upper limit of the IG-TTD can be seen for all data sets. The CLIVAR A13.5 data show that the northern data are in the application range of the IG-TTD, whereas ANT-XXVIII/3 data cannot be applied to the model. The SWEDARP data show a scattered and indistinct structure with no clear trend. The dashed black lines indicate the sensitivity limit that is explained in Sect. 4.4.

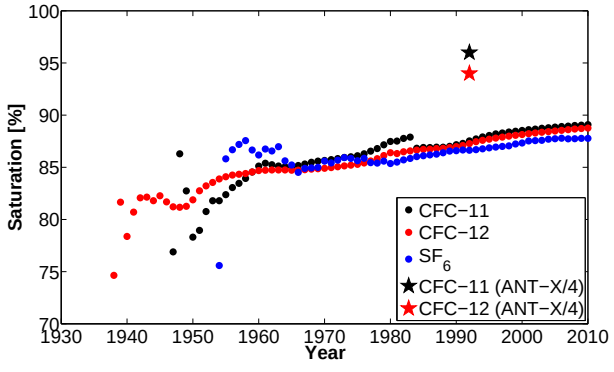

Figure 8. Yearly maximum surface undersaturation of CFC-12, CFC-11 and SF_6 between 50 and 68° S and between 30° W and 20° E in the Southern Ocean. The surface saturation was relatively similar for all three transient tracers over the last 30 years. The black and red stars indicate the CFC-12 and CFC-11 mean surface saturations that were obtained during the ANT-X/4 cruise in 1992.

trend, with a mean bottom concentration of 0.15 ppt. The water layer above the AABW consists of Circumpolar Deep Water (CDW), which is split into an upper and lower part (UCDW, LCDW) and mixes with southwards-propagating NADW. The CFC concentrations are 4–20 ppt of CFC-12 and 2–8 ppt of CFC-11 between 1500 and 3000 m and between 40 and 50° S. Here again, SF_6 is barely detectable. Similar for all three tracers is the decreasing concentration from a nearly saturated surface layer to low tracer concentrations in intermediate layers with concentration gradients corresponding to the shape of the pycnocline.

Applying the IG-TTD model to the tracer couples CFC-12–SF_6 and CFC-11–SF_6, it is shown that the model (i.e., the Δ / Γ ratios) can be constrained for most of the intermediate depths and that both tracer couples yield similar results (Fig. 12). The indicated north–south trend of Fig. 7b and c can be seen by the increasing Δ / Γ ratios between 37 and 46° S until they reach the upper limit of the IG-TTD. Based on the theory of the IG-TTD model, these high ratios describe more diffusive water masses. However, according to Holzer and Primeau (2012), it should also be taken into ac-

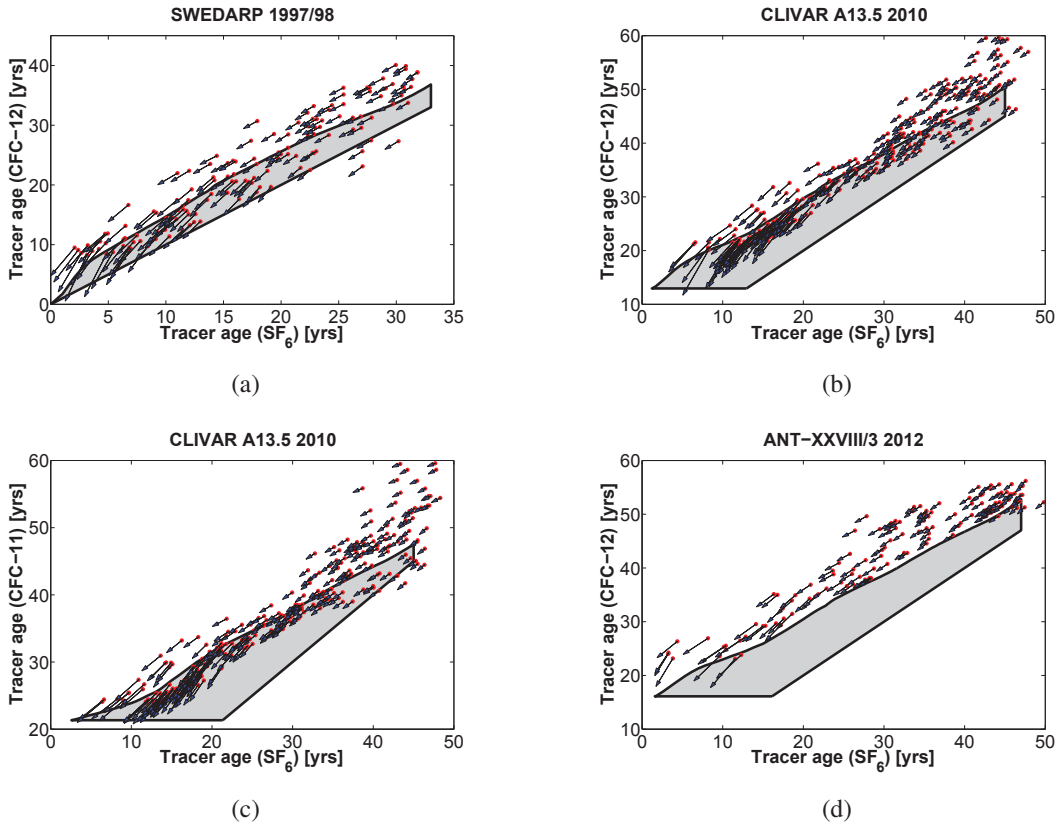

Figure 9. Changes in the tracer age relationships based on saturation corrections. The red dots indicate the relationship of the original and the arrowheads of the saturation-corrected data. The data sets are similar to Fig. 7 of **(a)** SWEDARP, **(b, c)** CLIVAR A13.5 and **(d)** ANT-XXVIII/3. The saturation correction affects the Δ / Γ ratios only to minor extent for a SF_6 tracer age > 20 years, but shows a shift towards lower Δ / Γ ratios below this limit.

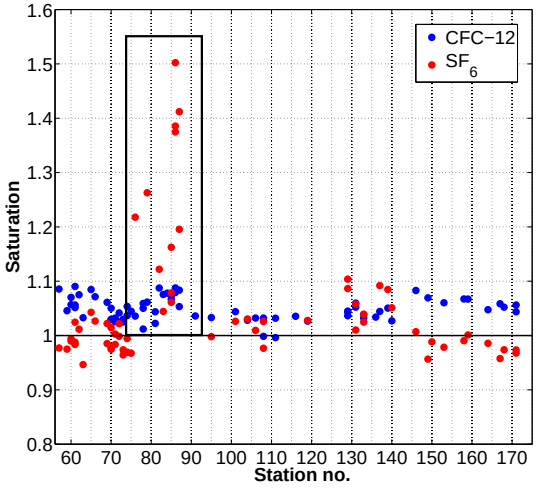

Figure 10. Surface saturation of CFC-12 and SF_6 during the ANT-XXVIII/3 cruise in 2012. SF_6 shows significant supersaturation 1 day after heavy weather conditions with wind speeds between 20 and 25 $m\,s^{-1}$ (black box).

count that different mixing mechanisms (e.g., diapycnal mixing) change water mass characteristics in a way that cannot by determined with the IG-TTD and that causes high Δ / Γ ratios in the transition area. Figure 13 shows the salinity of the CLIVAR A13.5 section where black dots indicate tracer data, which is within the validity area of the IG-TTD. Similar to the findings of Holzer and Primeau (2012) and Waugh et al. (2013), the southern IG-TTD limit is near the Subantarctic Front (SAF), which is shown by the surface salinity gradient at $\approx 46°$ S. Furthermore, the corresponding low salinity layer of the Antarctic Intermediate Water (AAIW) denotes the vertical limiting layer.

Comparing the transition zone of the detection limit of SF_6 between 5° N and 20° S in Fig. 7c with the related area in Fig. 12, it can be seen that this transition is characterized by very low Δ / Γ ratios (< 0.2). This feature corresponds to the shifted data points towards lower Δ / Γ ratios for a SF_6 tracer age > 32 years in Fig. 7b and c. Here again, these low ratios correspond to specific characteristics of low tracer concentrations rather than describing a highly advective behavior of water masses in this area. This effect can also be found south of the SAF, as indicated by the isolated occurring low Δ / Γ

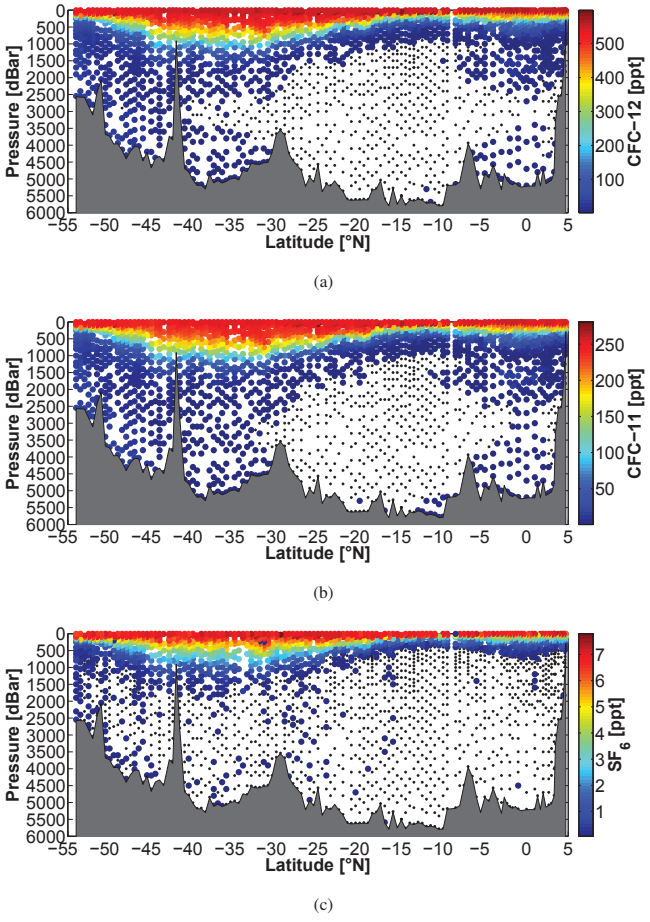

Figure 11. Transient tracer concentrations of the CLIVAR A13.5 section along the Greenwich Meridian in 2010 of **(a)** CFC-12, **(b)** CFC-11 and **(c)** SF_6 in ppt. The black dots indicate measurements with concentrations below the detection limit.

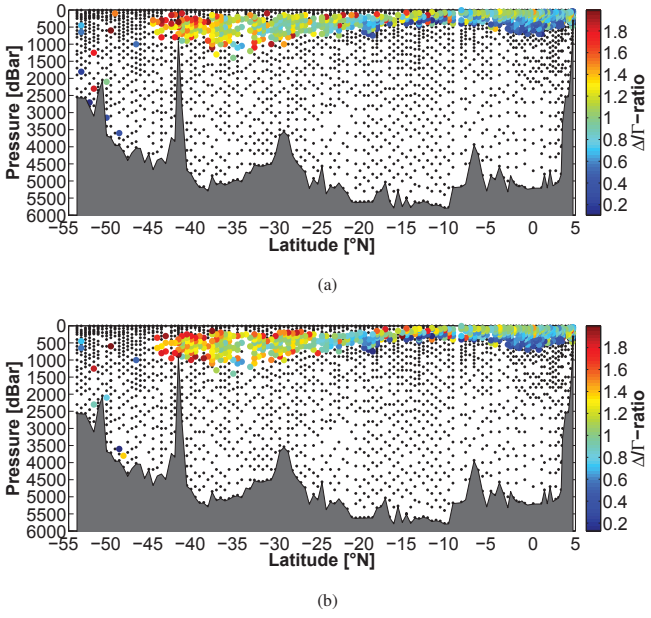

Figure 12. Constrained Δ / Γ ratios of the CLIVAR A13.5 section along the Greenwich Meridian in 2010 using the tracer couples **(a)** CFC-12/SF_6 and **(b)** CFC-11/SF_6. The black dots indicate data below the detection limit and data outside the application range of the IG-TTD.

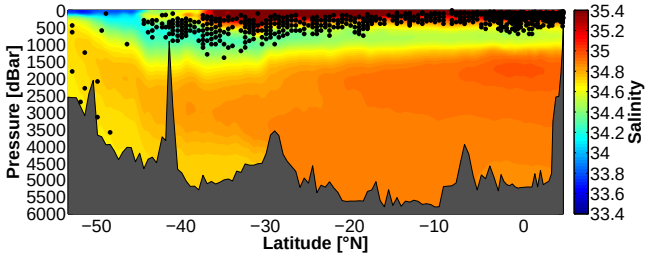

Figure 13. Salinity section of the CLIVAR A13.5 section along the Greenwich Meridian in 2010. The black dots indicate data within the application range of the IG-TTD (i.e., constrainable data points). The IG-TTD-limiting SAF can be identified by the salinity drop at $\approx 46°$ S and the AAIW by the low-salinity layer originating south of the SAF.

ratios. This specific limit can be estimated using the tracer order plot (Fig. 3). The CFCs and SF_6 show relatively linear decreasing trends of the relative tracer concentration that flatten out for higher tracer age. This causes a high tracer age sensitivity to changes in concentration and the transition between the linear trend, and the flattening is defined as the tracer age limit. The corresponding tracer concentrations are described as a sensitivity limit that replaces the LOD as the limit of the validity area (see the black dotted lines in Fig. 7b and c). The sensitivity limit changes with time, i.e., depends on the atmospheric histories of the tracers. The sensitivity limit in 2010 was ≈ 32 years for SF_6 (0.6 ppt or ≈ 0.22 fmol kg^{-1}) and ≈ 50 years for CFC-11 (10 ppt or ≈ 0.22 pmol kg^{-1}) and CFC-12 (30 ppt or ≈ 0.17 pmol kg^{-1}). Figure 7b and c show that the smallest sensitivity limit, defined by SF_6, determines the validity area. The sensitivity limit of radioactive transient tracers cannot be determined in a similar way, since the relative tracer concentrations depend on decay functions instead of atmospheric histories. A tracer couple usually includes a non-radioactive tracer (except for ^{39}Ar–^{14}C) and it can be assumed that the sensitivity limit of CFCs or SF_6 is smaller than that of radioactive tracers. Therefore, the sensitivity limits of radioactive transient tracers do not change the validity area.

The non-constrainable data points in Fig. 12 of the surface layer are related to the atmospheric concentration limits of the CFCs, which prohibit any statements about age-related results. The remaining constrained data points have Δ / Γ ratios between 0.8 and 1.2, i.e., around the unity ratio of 1.0.

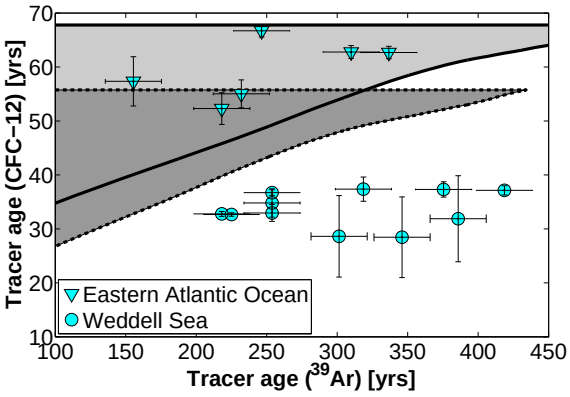

Figure 14. Tracer age relationship of CFC-12 and ^{39}Ar. The CFC-12 data of the CLIVAR A13.5 cruise (validity area of 2010, light grey area) were interpolated to the isopycnals of the ^{39}Ar data of the eastern Atlantic Ocean (cyan triangles). Accordingly, the CFC-12 data of the ANT-X/4 cruise (validity area of 1992, dark grey area) were interpolated to the ^{39}Ar data of the Weddell Sea (cyan dots). The validity areas of 1992 (dark grey area) and 2010 (light grey area) correspond to the year of sampling of CFC-12. Data from the eastern Atlantic Ocean (triangles) can be found within the application range of the IG-TTD, whereas most of the data from the Weddell Sea remain outside.

4.5 Argon-39 investigations

The tracer couple combinations with SF_6 have shown that deep water cannot be investigated due to the absence of this tracer or the bias of IG-TTD results near the detection limit. Therefore, we interpolated CFC-12 data from the northern part of the CLIVAR cruise and the southern part of the ANT-X/4 cruise to the corresponding isopycnals of the ^{39}Ar data in the eastern Atlantic and the Weddell Sea, respectively (Table 2). These data were then applied to the validity area of the CFC-12–^{39}Ar tracer couple of 1992 and 2010 (Fig. 14). It can be seen that the IG-TTD could be constrained in the eastern Atlantic (triangles in the light grey area of 2010) and remains outside of the validity area for the Weddell Sea (dots in the dark grey area of 1992). The error range of ^{39}Ar was assumed to be ± 5 %, which is ≈ 20 years in tracer age, whereas the error range of CFC-12 is related to the standard deviation of the interpolated concentrations (see the error bars in Fig. 14). Similar to the tracer couples including SF_6, the north–south trend of the tracer data can be identified. Furthermore, this approach shows that ^{39}Ar data are a promising alternative for deep water analyses.

5 Conclusions

Transient tracers in combination with the IG-TTD are a powerful tool to investigate ocean ventilation. To analyze well-ventilated water masses, SF_6 and δ^3H should be used due to the young atmospheric history and high decay rate, respectively. CFCs have declined in the atmosphere since the late 1990s, which leads to ambiguous results in tracer age and mean age for values above this atmospheric concentration limit. This restriction only affects surface waters and to a certain extent intermediate waters at present, so that CFC data still play a major role in the analysis of deep water ventilation. ^{39}Ar has a low decay rate, which provides a larger time range than CFC-12. It is thus a useful tracer for less ventilated water masses, e.g., deep ocean basins in the Pacific Ocean. The recent developments of the ATTA method provide a more adequate sampling and measurement of ^{39}Ar than in the past, so that ^{39}Ar will become more focused in future work. The ambiguous or unknown boundary conditions of radiocarbon complicate the application of the IG-TTD model, and thus ^{14}C is not recommended for use in combination with the IG-TTD.

The IG-TTD can be empirically constrained by using a transient tracer couple. Each tracer couple has a specific validity area, e.g., CFC-12 and SF_6 for intermediate and CFC-12 and ^{39}Ar for deep water masses. The new concept of validity areas provides information about the application range of a specific tracer couple and the limits of the IG-TTD. Data sets of transient tracer surveys in the ocean can simply be checked against validity areas to ascertain whether the IG-TTD can be applied or not. The radioactive transient tracers have constant validity areas in time, which is based on their steady boundary conditions. The chronological transient tracers depend on their atmospheric history and thus a changing boundary condition that has direct impacts on the determination of the validity area. Tracer saturation is an important factor with possible large impacts on Δ / Γ ratios and thus also the mean age. Specific corrections for the saturation of CFC-11, CFC-12 and SF_6 can be taken from a surface saturation model provided by Shao et al. (2013).

The field data application of the CLIVAR A13.5 cruise in 2010 indicates that Δ / Γ ratios, which are based on the tracer couples CFC-11/SF_6 and CFC-12/SF_6, do not necessarily correspond to the advective/diffusive behavior of a water parcel, but rather describe the transition between the validity area and the different limits of the IG-TTD. The limits of the IG-TTD in the Southern Ocean are defined by the SAF as the southern limit and, as a consequence, the AAIW is the limiting water layer. The constrained Δ / Γ ratios are between 0.8 and 1.2, which is close to the commonly applied ratio of 1.0. The IG-TTD can be applied to large parts in the ocean, but reaches its limits where complex ventilation patterns prevail, e.g., in the Southern Ocean. Thus, other models are required to analyze such ventilation processes, e.g., the maximum entropy method by Holzer and Primeau (2012) or the linear combination of two IG-TTDs (Waugh et al., 2003).

Acknowledgements. This work was supported by the Deutsche Forschungsgemeinschaft (DFG) in the framework of the "Antarctic Research with comparative investigations in Arctic ice areas" priority program by a grant to T. Tanhua and M. Hoppema: Carbon and transient tracers dynamics: A bi-polar view on Southern Ocean eddies and the changing Arctic Ocean (TA 317/5, HO 4680/1). Partial support to T. Tanhua and M. Hoppema was received from EU FP7 project CARBOCHANGE: "Changes in carbon uptake and emissions by oceans in a changing climate" (European Community's 7th Framework Programme, grant agreement no. 264879). Support for J. Bullister was provided by NOAA's Climate Program Office. This is PMEL contribution no. 4316. We are grateful to the Alfred-Wegener-Institut for participation in the "Eddy Pump" *Polarstern* cruise. We are happy to acknowledge the great support by the master and crew of *Polarstern*, the chief scientist and the scientific party. Special thanks goes to Boie Bogner for his technical support during the ANT-XXVIII/3 cruise and David Wisegarver on the CLIVAR A13.5 cruise.

The article processing charges for this open-access publication were covered by a Research Centre of the Helmholtz Association.

Edited by: D. Stevens

References

Aeschbach-Hertig, W.: Helium und Tritium als Tracer für physikalische Prozesse in Seen, PhD thesis, ETH Zürich, Zürich, Switzerland, 1994.

Bolin, B. and Rodhe, H.: A note on the concepts of age distribution and transit time in natural reservoirs, Tellus, 25, 58–62, doi:10.1111/j.2153-3490.1973.tb01594.x, 1973.

Broecker, W. and Peng, T.: Gas exchange rates between air and sea, Tellus, 26, 21–35, doi:10.1111/j.2153-3490.1974.tb01948.x, 1974.

Bullister, J.: Atmospheric Histories (1765–2015) for CFC-11, CFC-12, CFC-113, CCl_4, SF_6 and N_2O, Carbon Dioxide Information Analysis Center, http://cdiac.ornl.gov/ftp/oceans/CFC_ATM_Hist/CFC_ATM_Hist_2015, 2015.

Bullister, J. and Key, R.: CLIVAR/Carbon A13.5 Cruise Report, CCHDO, http://cchdo.ucsd.edu/data/b/c34715/a13-5_33RO20100308do.txt, 2010.

Bullister, J. and Weiss, R.: Determination of CCl_3F and CCl_2F_2 in seawater and air, Deep-Sea Res., 35, 839–853, doi:10.1016/0198-0149(88)90033-7, 1988.

Bullister, J. and Wisegarver, D.: The shipboard analysis of trace levels of sulfur hexafluoride, chlorofluorocarbon-11 and chlorofluorocarbon-12 in seawater, Deep-Sea Res., 55, 1063–1074, doi:10.1016/j.dsr.2008.03.014, 2008.

CLSI: Protocols for Determination of Limits of Detection and Limits of Quantification, approved Guideline, CLSI document EP17, Clinical and Laboratory Standards Institute, Wayne, PA USA, 2004.

CNSC: Investigation of the Environmental Fate of Tritium in the Atmosphere, INFO-0792, minister of Public Works and Government Services Canada, Canadian Nuclear Safety Commission, 2009.

Cossairt, J. D.: Background levels of tritium, Environmental Protection Note, 28, 1–4, 2012.

DeGrandpre, M. D., Koertzinger, A., Send, U., Wallace, D. W. R., and Bellerby, R. G. J.: Uptake and sequestration of atmospheric CO_2 in the Labrador Sea deep convection region, Geophys. Res. Lett., 33, L21S03, doi:10.1029/2006GL026881, 2006.

Dickson, A., Sabine, C., and Christian, J.: Guide to Best Practices for Ocean CO_2 Measurements, PICES Special Publication 3, 191 pp., 2007.

Dreisigacker, E. and Roether, W.: Tritium and ^{90}Sr in North Atlantic surface water, Earth Planet. Sc. Lett., 38, 301–312, 1978.

Engelkemeir, A. G., Hamill, W. H., Inghram, M. G., and Libby, W. F.: The half-life of radiocarbon (^{14}C), Phys. Rev., 75, 1825, doi:10.1103/PhysRev.75.1825, 1949.

Grasshoff, K., Kremling, K., and Ehrhardt, M.: Methods of Seawater Analysis, Wiley-VCH, Weinheim, 1999.

Haine, T. W. N. and Richards, K. J.: The influence of the seasonal mixed layer on oceanic uptake of CFCs, J. Geophys. Res.-Oceans, 100, 10727–10744, doi:10.1029/95JC00629, 1995.

Hall, T. M. and Plumb, R. A.: Age as a diagnostic of stratospheric transport, J. Geophys. Res., 99, 1059–1070, 1994.

Holzer, M. and Primeau, F. W.: Improved constraints on transit time distributions from argon 39: A maximum entropy approach, J. Geophys. Res.-Oceans, 115, C12021, doi:10.1029/2010JC006410, 2012.

Huhn, O., Rhein, M., Hoppema, M., and van Heuven, S.: Decline of deep and bottom water ventilation and slowing down of anthropogenic carbon storage in the Weddell Sea, Deep-Sea Res., 76, 66–84, doi:10.1016/j.dsr.2013.01.005, 2013.

Jenkins, W. J.: Tritium-Helium Dating in the Sargasso Sea: A Measurement of Oxygen Utilization Rates, Science, 196, 291–292, doi:10.1126/science.196.4287.291, 1977.

Jiang, W., Williams, W., Bailey, K., Davis, A., Hu, S., Lu, Z., O'Connor, T., Purtschert, R., Sturchio, N., Sun, Y., and Mueller, P.: ^{39}Ar Detection at the 10^{-16} Isotopic Abundance Level with Atom Trap Trace Analysis, Phys. Rev. Lett., 106, 103001, doi:10.1103/PhysRevLett.106.103001, 2011.

Klatt, O., Roether, W., Hoppema, M., Bulsiewicz, K., Fleischmann, U., Rodehacke, C., Fahrbach, E., Weiss, R. F., and Bullister, J. L.: Repeated CFC sections at the Greenwich Meridian in the Weddell Sea, J. Geophys. Res.-Oceans, 107, 3030, doi:10.1029/2000JC000731, 2002.

Krane, K.: Introductory Nuclear Physics, John Wiley and Sons Inc., New York, USA, p. 796, 1987.

Krysell, M., Fogelqvist, E., and Tanhua, T.: Apparent removal of the transient tracer carbon tetrachloride from anoxic seawater, Geophys. Res. Lett., 21, 2511–2514, doi:10.1029/94GL02336, 1994.

Law, C. S., Watson, A. J., and Liddicoat, M. I.: Automated vacuum analysis of sulphur hexafluoride in seawater: derivation of the atmospheric trend (1970–1993) and potential as a transient tracer, Mar. Chem., 48, 57–69, 1994.

Lee, B.-S., Bullister, J. L., and Whitney, F. A.: Chlorofluorocarbon CFC-11 and carbon tetrachloride removal in Saanich Inlet, an intermittently anoxic basin, Mar. Chem., 66, 171–185, doi:10.1016/S0304-4203(99)00039-0, 1999.

Lee, B.-S., Bullister, J. L., Murray, J. W., and Sonnerup, R. E.: Anthropogenic chlorofluorocarbons in the Black Sea and the Sea of

Marmara, Deep-Sea Res. Pt. I, 49, 895–913, doi:10.1016/S0967-0637(02)00005-5, 2002.

Lemke, P.: The expedition ANTARKTIS X/4 of RV "Polarstern" in 1992, Reports on polar and marine research, Alfred Wegener Institute for Polar and Marine Research, Bremerhaven, Germany, 140, 1994.

Liang, J.-H., Deutsch, C., McWilliams, J. C., Baschek, B., Sullivan, P. P., and Chiba, D.: Parameterizing bubble-mediated air-sea gas exchange and its effect on ocean ventilation, Global Biogeochem. Cy., 27, 894–905, doi:10.1002/gbc.20080, 2013.

Libby, W. F.: Radiocarbon Dating, University of Chicago Press, Chicago, USA, 1955.

Loosli, H. H.: A dating method with ^{39}Ar, Earth Planet. Sc. Lett., 63, 51–62, 1983.

Lu, Z.-T., Schlosser, P., Smethie Jr., W. M., Sturchio, N. C., Fischer, T. P., Kennedy, B. M., Purtschert, R., Severinghaus, J. P., Solomon, D. K., Tanhua, T., and Yokochi, R.: Tracer applications of noble gas radionuclides in the geosciences, Earth-Sci. Rev., 138, 196–214, doi:10.1016/j.earscirev.2013.09.002, 2014.

Minschwaner, K., Hoffmann, L., Brown, A., Riese, M., Müller, R., and Bernath, P. F.: Stratospheric loss and atmospheric lifetimes of CFC-11 and CFC-12 derived from satellite observations, Atmos. Chem. Phys., 13, 4253–4263, doi:10.5194/acp-13-4253-2013, 2013.

Orr, J. C., Fabry, V. J., Aumont, O., Bopp, L., Doney, S. C., Feely, R. A., Gnanadesikan, A., Gruber, N., Ishida, A., Joos, F., Key, R. M., Lindsay, K., Maier-Reimer, E., Matear, R., Monfray, P., Mouchet, A., Najjar, R. G., Plattner, G. K., Rodgers, K. B., Sabine, C. L., Sarmiento, J. L., Schlitzer, R., Slater, R. D., Totterdell, I. J., Weirig, M. F., Yamanaka, Y., and Yool, A.: Anthropogenic ocean acidification over the twenty-first century and its impact on calcifying organisms, Nature, 437, 681–686, doi:10.1038/nature04095, 2005.

Ravishankara, A. R., Solomon, S., Turnipseed, A. A., and Warren, R. F.: Atmospheric lifetimes of long-lived halogenated species, Science, 259, 194–199, doi:10.1126/science.259.5092.194, 1993.

Rodriguez, J.: Beiträge zur Verteilung von ^{39}Ar im Atlantik, PhD thesis, University of Bern, Switzerland, 1993.

Roether, W.: On oceanic boundary conditions for tritium, on tritiugenic ^{3}He, and on the tritium-^{3}He age concept, in: Oceanic Circulation Models: Combining Data and Dynamics, edited by: Anderson, D. and Willebrand, J., Vol. 284 of NATO ASI Series, Springer, the Netherlands, 377–407, doi:10.1007/978-94-009-1013-3_12, 1989.

Roether, W., Schlosser, P., Kuntz, R., and Weiss, W.: Transient-tracer studies of the thermohaline circulation of the Mediterranean, Reports in Meteorology and Oceanography, 41, 291–317, 1992.

Roether, W., Jean-Baptiste, P., Fourré, E., and Sültenfuß, J.: The transient distributions of nuclear weapon-generated tritium and its decay product ^{3} He in the Mediterranean Sea, 1952–2011, and their oceanographic potential, Ocean Sci., 9, 837–854, doi:10.5194/os-9-837-2013, 2013.

Sabine, C. L. and Tanhua, T.: Estimation of anthropogenic co_2 inventories in the ocean, Annu. Rev. Mar. Sci., 2, 175–198, doi:10.1146/annurev-marine-120308-080947, 2010.

Schlitzer, R. and Roether, W.: A meridional ^{14}C and ^{39}Ar section in Northeast Atlantic deep water, J. Geophys. Res., 90, 6945–6952, 1985.

Schlosser, P., Bayer, R., Bönisch, G., Cooper, L. W., Ekwurzel, B., Jenkins, W. J., Khatiwala, S., Pfirman, S., and Smethie, W. M.: Pathways and mean residence times of dissolved pollutants in the ocean derived from transient tracers and stable isotopes, Sci. Total Environ., 237–238, 15–30, doi:10.1016/S0048-9697(99)00121-7, 1999.

Schneider, A., Tanhua, T., Koertzinger, A., and Wallace, D. W. R.: High anthropogenic carbon content in the eastern Mediterranean, J. Geophys. Res., 115, C12050, doi:10.1029/2010JC006171, 2010.

Schneider, A., Tanhua, T., Koertzinger, A., and Wallace, D. W. R.: An evaluation of tracer fields and anthropogenic carbon in the equatorial and the tropical North Atlantic, Deep-Sea Res. Pt. I, 67, 85–97, doi:10.1016/j.dsr.2012.05.007, 2012.

Schneider, A., Tanhua, T., Roether, W., and Steinfeldt, R.: Changes in ventilation of the Mediterranean Sea during the past 25 year, Ocean Sci., 10, 1–16, doi:10.5194/os-10-1-2014, 2014.

Shao, A. E., Mecking, S., Thompson, L., and Sonnerup, R. E.: Mixed layer saturations of CFC-11, CFC-12, and SF6 in a global isopycnal model, J. Geophys. Res.-Oceans, 118, 4978–4988, doi:10.1002/jgrc.20370, 2013.

Sonnerup, R., Mecking, S., and Bullister, J.: Transit time distributions and oxygen utilization rates in the Northeast Pacific Ocean from chlorofluorocarbons and sulfur hexafluoride, Deep-Sea Res., 72, 61–71, doi:10.1016/j.dsr.2012.10.013, 2013.

Stöven, T.: Ventilation processes of the Mediterranean Sea based on CFC-12 and SF_6 measurements, GEOMAR OceanRep, available at: http://oceanrep.geomar.de/id/eprint/13936 (last access: 14 October 2014), Diploma thesis, Christian-Albrechts-Universität zu Kiel, Kiel, Germany, 2011.

Stöven, T. and Tanhua, T.: Ventilation of the Mediterranean Sea constrained by multiple transient tracer measurements, Ocean Sci., 10, 439–457, doi:10.5194/os-10-439-2014, 2014.

Stuiver, M.: Variations in radiocarbon concentration and sunspot activity, J. Geophys. Res., 66, 273–276, doi:10.1029/JZ066i001p00273, 1961.

Tanhua, T., Olsson, K. A., and Fogelqvist, E.: A first study of SF_6 as a transient tracer in the Southern Ocean, Deep-Sea Res. Pt. II, 51, 2683–2699, doi:10.1016/j.dsr2.2001.02.001, 2004.

Tanhua, T., Olsson, K. A., and Jeansson, E.: Formation of Denmark Strait overflow water and its hydro-chemical composition, J. Mar. Syst., 57, 264–288, doi:10.1016/j.jmarsys.2005.05.003, 2005.

Tanhua, T., Waugh, D. W., and Wallace, D. W. R.: Use of SF_6 to estimate anthropogenic CO_2 in the upper ocean, J. Geophys. Res., 113, 2156–2202, doi:10.1029/2007JC004416, 2008.

Tanhua, T., Waugh, D. W., and Bullister, J. L.: Estimating changes in ocean ventilation from the early 1990s CFC-12 and late SF_6 measurements, Geophys. Res. Lett., 40, 927–932, doi:10.1002/grl.50251, 2013.

Tans, P. P., de Jong, A. F. M., and Mook, W. G.: Natural atmospheric ^{14}C variations and the Suess effect, Nature, 280, 826–828, doi:10.1038/280826a0, 1979.

Turner, D. R., Bertilsson, S., Fransson, A., and Pakhomov, E.: The SWEDARP 1997/98 marine expedition: overview, Deep-Sea Res. Pt. II, 51, 2543–2556, doi:10.1016/j.dsr2.2003.08.006, 2004.

Waugh, D. W., Vollmer, M. K., Weiss, R. F., Haine, T. W. N., and Hall, T. M.: Transit time distributions in Lake Issyk-Kul, Geophys. Res. Lett., 29, 841–844, doi:10.1029/2002GL016201, 2002.

Waugh, D. W., Hall, T. M., and Haine, T. W. N.: Relationships among tracer ages, J. Geophys. Res., 108, 3138, doi:10.1029/2002JC001325, 2003.

Waugh, D. W., Haine, T. W. N., and Hall, T. M.: Transport times and anthropogenic carbon in the subpolar North Atlantic Ocean, Deep-Sea Res., 51, 1475–1491, 2004.

Waugh, D. W., Primeau, F., DeVries, T., and Holzer, M.: Recent changes in the ventilation of the Southern Oceans, Science, 339, 568–570, doi:10.1126/science.1225411, 2013.

Waugh, D. W., Hall, T. M., McNeil, B. I., Key, R., and Matear, R. J.: Anthropogenic CO_2 in the oceans estimated using transit time distributions, Tellus B, 58, 376–389, 2006.

Whitworth, T. and Nowlin, W.: Water masses and currents of the Southern Ocean at the Greenwich Meridian, J. Geophys. Res.-Oceans, 92, 6462–6476, doi:10.1029/JC092iC06p06462, 1987.

Wolf-Gladrow, D.: The expedition of the research vessel "Polarstern" to the Antarctic in 2012 (ANT-XXVIII/3), Reports on polar and marine research, 661, 2013.